

國立臺灣大學生物環境資源暨農學院

生物環境系統工程學研究所

碩士論文

Department of Bioenvironmental Systems Engineering

College of Bioresources and Agriculture

National Taiwan University

Master Thesis

都市街谷內噴霧降溫效果之模擬

A Numerical Study of the Temperature Reduction by
Water Spray Systems within Urban Street Canyons

李映辰

Ying-Chen Lee

指導教授：謝正義 博士

Advisor：Cheng-I Hsieh, Ph.D.

中華民國 106 年 6 月

June 2017



Acknowledgement



首先要感謝我的指導教授—謝正義老師，從物理系轉來生工所以及碩士班兩年的期間，老師以開放的方式讓我們發揮所長，以嚴謹的方式指導我們完成碩士論文；也謝謝朱佳仁老師、陳明志老師、張倉榮老師抽空幫我口試，並給我許多寶貴的意見，在口試期間聽到不少實用的建議及可以改進的方向。

謝謝研究室的大家，承駿學長、政崴和俊德，研究室裡大大小小的事情，都能有效率的一起解決，這段期間是非常難得的合作經驗。在研究的方向還有進度上也感謝你們督促我給我建議。也感謝常常陪伴給予打氣的朋友，在這段期間的鼓勵及各式各樣的聊天紓壓。

最後要謝謝家人，在接近口試的期間，常常熬夜看日出的那段日子，感謝家人一直注意我的身體健康，給予各種關心，是最強的後盾！



摘要

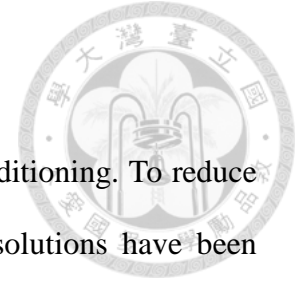
都市熱島效應使得都市空調需求劇烈增加，為了降低降溫的耗電需求，有許多研究探討除了冷氣以外的降溫方式，然而噴霧降溫被認為是眾多方法中較有效率且彈性的降溫方式。

噴霧顆粒與空氣的動量、能量、質量交換為二相流(two-phase flow)問題，可以利用計算流體力學的 Lagrange-Eulerian 耦合模型模擬。本研究利用水槽實驗驗證街谷內流場，搭配已被驗證的粒子模型，模擬噴霧在都市街谷內的降溫效果。本研究主要的目標為模擬在高濕度(相對溼度為 70% 及 80%)、不同街谷高寬比的街谷內降溫情形，以符合台北都會區夏季的平均濕度情況。

模擬結果顯示不同街谷高寬比下，當相對溼度大於 70%時，小顆粒的水珠噴出後會在短時間使空氣達到飽和，而大顆粒的水珠亦會使噴霧正下方空氣非常接近飽和，隨著噴霧高度增高(由 2.5 公尺增高至 3.5 公尺)，噴霧正下方空氣會達到飽和，並降溫至濕球溫度，也就是蒸發降溫的極限溫度。因此在台北都會區內，水珠粒子與噴霧高度並非需要考量的變因。由於都市街谷內風速較慢，無法帶走水珠粒子以及降溫後的空氣，因此受到噴霧影響最大的區域就是噴霧下方；另外在窄街谷內，由於冷空氣較容易聚集在街道內，因此街道中央的人可能可以感受到噴霧降溫的效果。

關鍵字：都市街谷、噴霧降溫系統、熱舒適度、二項流(two-phase flow)、Lagrangian-Eulerian 模型。

Abstract



Urban heat islands rapidly increase energy demand for air conditioning. To reduce the energy demand for cooling the environment, some possible solutions have been studied and applied. Among these methods, the water spray system is considered most effective and flexible with its dynamic controls. To simulate the cooling effect of water spray system, numerical simulation with Computational Fluid Dynamics (CFD) is used. This simulation was validated with water channel and wind tunnel experiments.

The goal of this study is to simulate the cooling effect in the street canyon with different aspect ratio in high relative humidity (70% and 80%) environment, which is often the case in Taipei city.

The results showed that if relative humidity is larger than 70%, the air cooled by small water droplets was easily saturated. Large water droplets almost saturated the air just under the nozzles. If the nozzle height was increased from 2.5 m to 3.5 m, the air under the nozzles was completely saturated, and reached wet bulb temperature, which is the lowest bound of temperature. The coolest region is just below the nozzles because the wind in street canyon is too weak to blow the cold air away. However, in a narrow street, people may feel the cooling effect in the middle of the street because the accumulation of the cold air.

Keywords: Urban street canyon, water spray system, thermal comfort, two phase flow, Lagrangian-Eulerian model.

Contents



Acknowledgement.....	I
摘要.....	II
Abstract.....	III
Contents	IV
List of Figures.....	VI
List of Tables	IX
1. Introduction	1
2. Methods	4
2.1 Mathematical model	4
2.2 Computational geometry and grid	6
2.3 Boundary conditions.....	7
2.4 Droplet and spray nozzle characteristic.....	9
2.5 Parametric analysis.....	10
2.6 Model validation.....	11
2.6.1 Validation of flow field in urban street canyon	11
2.6.2 Evaporation cooling validation.....	12
3. Results and discussion.....	15
3.1 Cooling effect with different aspect ratio and relative humidity.....	15
3.2 Effects of particle size and relative humidity	17
3.3 Effects of height of spray nozzles.....	19
4. Conclusions	19
Appendix	22
A.1 Governing equations of continuous phase.....	22



A.2 Governing equations of discrete phase (water droplets)..... 25

A.3 The derivation of wet bulb temperature..... 27

A.4 Extra cases 28

 A.4.1 Nozzles set on one side (left side or right side) of the street 28

 A.4.2 RH = 60% 28

Reference 30

Table 32

Figure..... 36

List of Figures

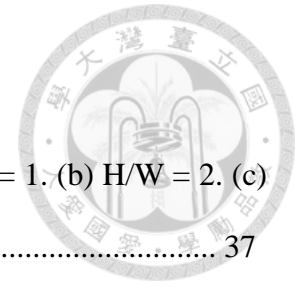


Figure 1 Computational domain for a street canyon. (a) $H/W = 1$. (b) $H/W = 2$. (c) $H/W = 3$ 37

Figure 2 The vertical profile of the normalized horizontal velocity (u) at $x/W = 0.5$ and $y = 0$ for different mesh sizes in the urban street canyon. u_r is reference velocity which is set to be 4 m/s. (a) $H/W = 1$. (b) $H/W = 2$. (c) $H/W = 3$ 39

Figure 3 Computational domain and meshing. (a) $H/W = 1$. (b) $H/W = 2$. (c) $H/W = 3$ 41

Figure 4 (a) View of a group of spray nozzles. (b) View of the urban street canyon with spray systems set in position $(x, z) = (1, 2.5)$ and $(x, z) = (14, 2.5)$. The y position of the spray nozzle are $\pm 1.5, \pm 1, \pm 0.5, 0$ 42

Figure 5 (a) Mass distribution with $D = 369 \mu m$. (b) Number distribution with $D = 369 \mu m$. (c) Mass distribution with $D = 20 \mu m$. (d) Number distribution with $D = 20 \mu m$ 44

Figure 6 Velocity field in urban street canyon without spray system. (a) $H/W = 1$. (b) $H/W = 2$. (c) upper region of $H/W = 2$. (d) lower region of $H/W = 2$ 47

Figure 7 Normalized vertical velocity as a function of normalized height at an upstream position ($x/W = 0.125$), middle position ($x/W = 0.5$) and downstream position ($x/W = 0.875$). U_t is the x direction velocity just above the top of the building. (a) $H/W = 1$. (b) $H/W = 2$ 48

Figure 8 Comparison of calculated (CFD) and measured (exp) result. (a) DBT. (b) humidity ratio. 49

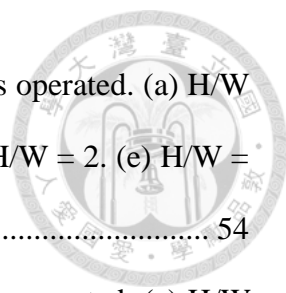


Figure 9 velocity field in the street canyon before spray systems operated. (a) H/W = 1. (b) H/W = 2. (c) upper region of H/W = 2. (d) lower region of H/W = 2. (e) H/W = 3. (f) upper region of H/W = 3. (g) lower region of H/W = 3. 54

Figure 10 velocity field in the street canyon after spray systems operated. (a) H/W = 1. (b) H/W = 2. (c) H/W = 3. 56

Figure 11 Temperature contours in the street canyon on the plane: $y = 0$ when $t = 5$ (sec) The black cross indicates the position of water spray systems. (a) Case 1.1 (H/W = 1). (b) Case 2.1 (H/W = 2). (c) Case 3.1 (H/W = 3). 58

Figure 12 Temperature contours in the street canyon on the plane: $y = 0$ when steady state reached. The black cross indicates the position of water spray systems. (a) Case 1.1 (H/W = 1, RH = 70%). (b) Case 2.1 (H/W = 2, RH = 70%). (c) Case 3.1 (H/W = 3, RH = 70%). (d) Case 1.2 (H/W = 1, RH = 80%). (e) Case 2.2 (H/W = 2, RH = 80%). (f) Case 3.2 (H/W = 3, RH = 80%). 61

Figure 13 Temperature profile on the line: $y = 0$, $z = 1.5$ m with different aspect ratio and Relative humidity in Case 1.1 (H/W = 1, RH = 70%), Case 2.1 (H/W = 2, RH = 70%), Case 3.1 (H/W = 3, RH = 70%), Case 1.2 (H/W = 1, RH = 80%), Case 2.2 (H/W = 2, RH = 80%), Case 3.2 (H/W = 3, RH = 80%). The background temperature is 35 °C and the normalized distance between the nozzles and building are 0.07, 0.1 and 0.2 for H/W = 1, 2, 3 respectively. 62

Figure 14 Temperature contour in Case 2.1 in the street canyon on x-y plane where height is 1.5 meters ($z = 1.5$). Dotted line shows the positions of spray nozzles (a) after 5 seconds. (b) after 12.5 seconds. 63

Figure 15 Temperature contours on the plane: $y = 0$. (a) Case 2.1 ($D = 20 \mu\text{m}$). (b) Case 2.1.a ($D = 40 \mu\text{m}$). 64

Figure 16 Temperature profile on the line: $y = 0$, $z = 1.5$ m, in Case 2.1 ($D = 20\mu\text{m}$, $V_w = 15$ m/s, $m = 0.01$ kg/s) and Case 2.1a ($D = 369 \mu\text{m}$, $V_w = 22$ m/s, $m = 0.2$ kg/s). The background temperature is 35°C 65

Figure 17 Residence time of droplet particles on the plane: $y = 0$. The black cross indicates the position of water spray systems. (a) Case 2.1 ($D = 20 \mu\text{m}$). (b) Case 2.1a ($D = 369 \mu\text{m}$). 66

Figure 18 Temperature contours on the plane: $y = 0$. (a) Case 2.1 (RH = 70%). (b) Case 2.2 (RH = 80%). 67

Figure 19 Relative humidity contours on the plane: $y = 0$. (a) Case 2.1 (RH = 70%, $D = 20 \mu\text{m}$). (b) Case 2.2 (RH = 80%, $D = 20 \mu\text{m}$). (c) Case 2.1a (RH = 70%, $D = 369 \mu\text{m}$). (d) Case 2.2a (RH = 80%, $D = 369 \mu\text{m}$). 69

Figure 20 Temperature profiles on the line: $y = 0$, $z = 1.5$ m with different heights of spray nozzles ($h_s = 2.5, 3, 3.5$ m). The background temperature is 35°C 70

Figure 21 Temperature contours on the plane: $y = 0$. (a) Left side, $H/W = 1$. (b) Right side, $H/W = 1$. (c) Left side, $H/W = 2$. (d) Right side, $H/W = 2$ 72

Figure 22 Temperature profiles on the line: $y = 0$, $z = 1.5$ m with spray nozzles wet on the left side or the right side. The background temperature is 35°C . (a) $H/W = 1$. (b) $H/W = 2$ 73

Figure 23 Temperature contours on the plane: $y = 0$ in the cases with RH = 60%. (a) $H/W = 1$. (b) $H/W = 2$. (c) $H/W = 3$ 75



List of Tables

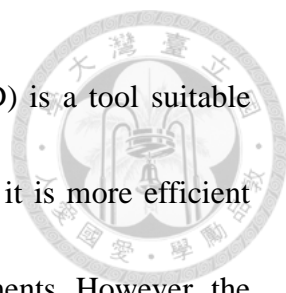
Table 1 Summary of parameters in the CFD model	32
Table 2 List of the parameters of the Cases.....	33
Table 3 The linear regression and root mean square error (RMSE) between experiment, the simulation results of Baik et al. (1999) and our predict results	34
Table 4 Average temperature on the line: $y = 0, z = 1.5$ m with different aspect ratio and relative humidity in Case 1.1 ($H/W = 1, RH = 70\%$), Case 2.1 ($H/W = 2, RH = 70\%$), Case 3.1 ($H/W = 3, RH = 70\%$), Case 1.2 ($H/W = 1, RH = 80\%$), Case 2.2 ($H/W = 2, RH = 80\%$), Case 3.2 ($H/W = 3, RH = 80\%$). The background temperature is $35\text{ }^{\circ}\text{C}$	35

1. Introduction



Urban heat islands form as a result of urbanization. It affects urban micrometeorology (Sarrat et al., 2006) and aggravates climate change, which has and will rapidly increase energy demand for air conditioning during the whole 2000-2100 period (Isaac and Vuuren, 2009).

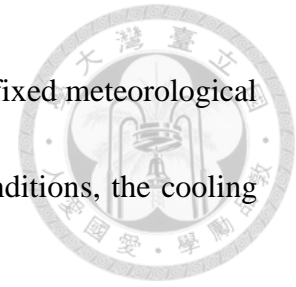
Some adaptations have been confirmed as valid for cooling urban areas or buildings such as green walls, green ponds (Alexandri and Jones, 2008), roof ponds (Runsheng and Erell, 2003), vegetation, increase of short wave reflectivity, and water spray systems. Among these, the water spray system is considered most effective and flexible with its dynamic controls in warm seasons while passive cooling systems such as vegetation and increase of short wave reflectivity also reduce temperature in cold weather. Furthermore, experiments conducted by Jain and Rao (1974) showed that roof spray systems performed better in reducing ceiling temperature than roof ponds did (15 °C and 13 °C respectively). Huang et al. (2011) conducted several experiments and proved the water spray system as being very effective since it reduced temperature by 5-7 °C under an ambient temperature of 35 °C and a relative humidity of 45 %. In spite of these benefits and universal application, studies on the cooling effect of water spray systems in urban environment are found to be relatively rare.



Numerical simulation with Computational Fluid Dynamics (CFD) is a tool suitable for studying momentum flow, energy flow, and particle flow since it is more efficient and cheaper than full-scale measurements and wind-tunnel experiments. However, the interaction between water droplets and air flow is rather complicated since it is a two phase flow, which takes into account the effect of energy exchange when droplets evaporate as well as momentum exchange between droplets and air flow. In order to simulate these effects, the Lagrangian-Eulerian (LE) model separates a two phase flow into the discrete phase part (Lagrangian model) and continuous phase part (Eulerian model), and these two models are coupled during the simulation. Several validation studies with small-scale and full-scale experimental data show that the Lagrangian-Eulerian model is reliable for simulating the two phase flow (Kang and Strand, 2013; Montazeri et al., 2015).

Although the LE model is widely used to simulate two phase flows, there are only a few studies applying this model to urban environments. Montazeri et al. (2017) simulated a water spray system in an urban landscape using the Lagrangian-Eulerian approach. The results showed that for a 9 kg/min water flow rate and a spray system installed at 3 m height, approximately a 7 °C temperature reduction is achieved at a height of 1.75 m in the courtyard, and heat stress is alleviated efficiently. However, the

study only simulated the cooling effect in a specific courtyard with fixed meteorological conditions. With different building geometry or meteorological conditions, the cooling effect may be quite different.



An urban street canyon is the space between buildings that line up continuously along both sides of a relatively narrow urban street. The wind velocity field (Baik and Kim, 1999) and pollutant dispersion (Chan et al., 2002) in urban street canyons have been studied. The results showed that the aspect ratio (building height divided by street width) is a crucial parameter that affects the velocity field and the dispersion of pollutant in the street canyon, in which more pollutants will be trapped in the street canyon with a higher aspect ratio. This phenomenon is likely to influence the outcome of the cooling effect in street canyon, since the cooling effect is affected by the dispersion of water droplets. Moreover, the water spray system is widely used to reduce air temperature in the urban canyons in night markets in Taipei as well as other south Asian cities during the summer. Most of the residential areas and night markets in Taipei are built in street canyons with aspect ratios larger than 1, which means that the wind velocity is lower in this region. With a high population density, low wind speed and high temperature in the summer, there is a high demand for cooling systems such as the water spray system to reduce temperatures in the street canyons in Taipei. However, its cooling effect has not yet been

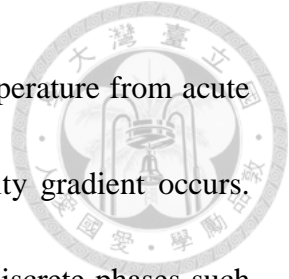


studied in a numerical manner. In order to contribute a wider application of water spray system, this study simulates the cooling effect of the water spray system in urban street canyon with manipulation of four variables: the aspect ratio of the street canyon, the relative humidity, droplet size and the height of the spray nozzles.

2. Methods

2.1 Mathematical model

All of the calculations were performed with ANSYS FLUENT (ANSYS Inc., 2013). The Eulerian part of the Lagrangian-Eulerian model contains continuous phases such as flow velocity field, temperature field and vapor concentration field. These are solved with 3D Reynolds-Averaged Navier-Stokes equations combined with the energy equation (see appendix A.1). Closure is obtained by the Re-Normalisation Group (RNG) k - ϵ model, as the simulation validation by Chan et al.(2002) suggested the RNG k - ϵ model as being the most optimum model compared to the standard k - ϵ model and the realizable k - ϵ model when simulating the flow field in a street canyon. Pressure-velocity coupling is performed with the Semi-Implicit Method for Pressure Linked Equations (SIMPLE). Second-order discretization schemes are used for all convection and viscous term and second-order implicit time integration is used for the temporal discretization.



Note that second-order implicit time integration can refrain the temperature from acute reducing caused by the accumulation of droplet when large velocity gradient occurs.

The Lagrangian part of the Lagrangian-Eulerian model, including discrete phases such as velocity, temperature and mass of water droplet are solved with the discrete phase model (DPM) implemented by ANSYS FLUENT. In this model, particles are accelerated by drag force (spherical drag law) and gravity force.

During the simulation, the DPM is turned off and the continuous phase flows are solved to steady a state by the 3D steady RNG k- ϵ model or unsteady RNG k- ϵ model first. Note that for the cases with $H/W = 2$ and $H/W = 3$, a steady state cannot be reached with the steady RNG k- ϵ model, therefore the unsteady k- ϵ model is used. After reaching the steady state, unsteady DPM is turned on and coupled with the 3D unsteady RNG k- ϵ model. The discrete phase model source term are updated after each continuous phase iteration. The time step size of continuous phase is 0.05 second, 15 iterations per time steps; 20 continuous phase iterations are done for each DPM iteration; particle time step size is 0.001 second and 0.05 second per injection. All of the time step sizes are decided with convergence tests.

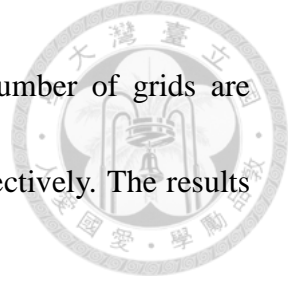


2.2 Computational geometry and grid

To simulate the effect of point sources in a nearly 2D flow field, the computational domain is set as a 3D long street canyon, with street length (L) much larger than street height (H), in order to get the same flow field as a 2D street canyon simulation.

Three types of street canyon ($H/W = 1, 2$ and 3) with geometry similar to real street canyons in Taipei were studied. The vertical (z direction) domain size was fixed to be 2 times of buildings height (H); the buildings widths were fixed to be the same as building height. The horizontal (x direction) domain size is equal to two times of building widths plus street width (W), i.e. the width between buildings, as shown in Figure 1. Street width (W) are 15 m, 10 m and 5 m for $H/W = 1, H/W = 2, H/W = 3$ respectively. The street lengths are fixed to be 150 m. The symmetry plane $y = 0$ is set in order to reduce computational time, that is, the domain of y direction actually computed is from $y = 0$ to $y = 75$ m.

The grid sizes are determined with a convergence test (Figure 2). The grids inside the street canyon need to be finer than on the outside; the grid size of cells adjacent to the buildings and street is set to be finer to model the effect of boundaries. Despite of the fine grid besides the boundaries, y^* for all boundaries in all cases were larger than 15. If y^* was smaller than 15, wall function will deteriorate (ANSYS Inc., 2013). The



number of divisions of W and H is 80x80, 70x70, 70x90; the number of grids are 295075, 241100 and 305350 for H/W = 1, H/W = 2, H/W = 3 respectively. The results of meshing are shown in Figure 3.

2.3 Boundary conditions

The leftmost boundary is a velocity inlet boundary and the boundary conditions for inlet velocity, kinetic energy (k) and kinetic energy dissipation rate (ϵ) are recommend by Baik et al. (1999):

$$U_i = U_r \left(\frac{z'}{H} \right)^{0.224} \quad (1)$$

$$W_i = 0 \quad (2)$$

$$k_i = 0.003 U_i^2 \quad (3)$$

$$\epsilon_i = \frac{C_\mu^{0.75} k_i^{1.5}}{\kappa z'} \quad (4)$$

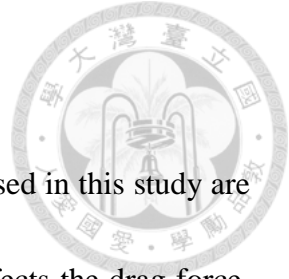
where U_i is the inlet horizontal velocity in x direction, W_i is the vertical velocity at the inlet boundary, $U_r (= 4 \text{ m/s})$ is the mean velocity at the boundary layer height (which is set to be H), κ is the von Kármán constant ($= 0.4$), C_μ is a constant ($= 0.0845$ in RNG k- ϵ model), and z' is the vertical distance from the top of the buildings.

The top and the rightmost boundaries are pressure outlet boundaries. The longitudinal end of the domain (plane: $y = 75 \text{ m}$) is a free-slip boundary restraining the



air from flowing outside to ensure the flow field in the street canyon close to 2D flow. The buildings and street were thermal adiabatic and were applied with standard wall function (Launder and Spalding, 1974). To reduce additional computational time caused by explicitly modeling the rough surface or fining the grids near the boundaries, the roughness height (k_s) and roughness constant (C_s) of these boundaries were set to be non-zero to model the effect of roughness of the boundaries. Roughness height of these boundaries were set to be 1.5; the roughness constant were set to be 0.5 with the validation in section 2.6.

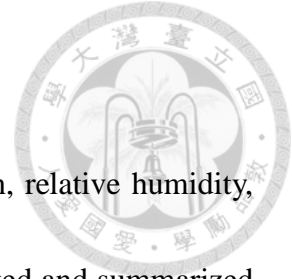
A model considering the interaction between the boundary and the discrete phase was needed. Since the temperature of the boundaries is below the boiling point of water, the “wall jet” boundary condition was not needed (ANSYS Inc., 2013). This study assumes that the droplets will be trapped on the wall, and the effect of the water film on the wall is neglected; thus an “escape” boundary condition in ANSYS FLUET discrete particle model was chosen so that droplets will disappear when they touch the wall. This assumption simplifies the calculation and ensures that the droplet will not be trapped in the air where the velocity is nearly zero.



2.4 Droplet and spray nozzle characteristic

All of the common CFD and nozzle characteristic parameters used in this study are summarized in Table 1. The water droplet size is crucial since it affects the drag force, gravity force and the residual time in the flow field. The droplet size distribution is determined by the Rosin-Rammler model, and the spread parameter $n = 3.5$ is determined by Montazeri et al. (2017). By the convergence test, 10 different diameters of particles are assumed to be injected from each droplet stream. The temperature of water droplet is 25 °C.

In this study, a cone spray model provided by ANSYS FLUENT 16.2 was used. The half-cone angle ($\alpha/2$) is 20 degree, the radius is 2 mm, and the total number of droplet streams is assumed to be 15 based on convergence test, i.e. there are 15 points of injection uniformly placed on the perimeter of the spray nozzle. There are two groups of nozzles, with 7 nozzles in each group. Two groups of nozzles are placed 1 meters beside two sides of buildings. In each group of nozzles, the distance between two adjacent nozzles follows the setting of Montazeri (2017), which is 0.5 m. The 7 nozzle group is installed in the same x and z coordinate, and the y coordinate is 0, ± 0.5 , ± 1.0 , ± 1.5 m, respectively as shown in Figure 4.



2.5 Parametric analysis

To analyze the effects of the aspect ratio of urban street canyon, relative humidity, particle size, and the height of spray nozzles, 10 cases were conducted and summarized in Table 2. The cases are numbered with the following rules:

1. The first number of the case indicates the aspect ratio ('1' for $H/W = 1$; '2' for $H/W = 2$; '3' for $H/W = 3$).
2. The second number of the case indicates the relative humidity ('1' for $RH = 70\%$; '2' for $RH = 80\%$).

If there is the third number for the case, it means that the mean particle size (\bar{D}) is larger ($\bar{D} = 369 \mu\text{m}$), and it also indicates the height of the spray nozzles (h_s) ('a' for $h_s = 2.5 \text{ m}$; 'b' for $h_s = 3 \text{ m}$; 'c' for $h_s = 3.5 \text{ m}$). For example, Case 2.1a is the case with $H/W = 1$, $RH = 70\%$, $\bar{D} = 369 \mu\text{m}$, $h_s = 2.5 \text{ m}$.

3. For the cases with $\bar{D} = 20 \mu\text{m}$, the minimum (D_{\min}) and maximum (D_{\max}) diameters of particles are $10 \mu\text{m}$, $60 \mu\text{m}$ respectively; the flow rate of water (\dot{m}) of each nozzle is 0.01 kg/s ; the velocity of water droplet (V_w) is 15 m/s , which follows the settings of Montazeri et al. (2017).
4. For the cases with $\bar{D} = 369 \mu\text{m}$, the minimum (D_{\min}) and maximum (D_{\max}) diameters of particles are $47 \mu\text{m}$, $518 \mu\text{m}$ respectively; the flow rate of water (\dot{m}) of



each nozzle is 0.2 kg/s; the velocity of water droplet (V_w) is 22 m/s, which follows the settings of Montazeri et al. (2015).

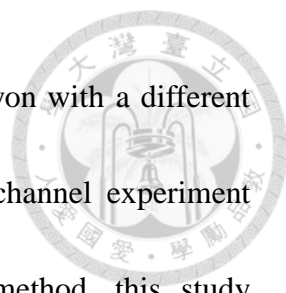
The mass and number distribution of different diameters of droplets in two kinds of cases ($\bar{D} = 369 \mu\text{m}$ and $\bar{D} = 20 \mu\text{m}$) were plotted in Figure 5.

To show which side (the left side or the right side) to set spray nozzles could have the better cooling effect and to show the the cooling effect when $\text{RH} = 60\%$, which are the often cases in Taiwan, extra cases are done (see Appendix A.4.2).

2.6 Model validation

2.6.1 Validation of flow field in urban street canyon

In this study, continuous phase reached steady state with 3D unsteady RNG k- ϵ model. The flow field of $H/W = 1$ and $H/W = 2$ on the plane: $y=0$ are shown in Figure 6. For $H/W = 1$, one clockwise vortexes in the street canyons is formed and for $H/W = 2$, two vortex with the upper one clockwise and the other counter-clockwise. The velocity magnitude of the upper vortex is lower than the velocity of inlet by approximately one order, and the lower vortex is lower than the velocity of the upper vortex by approximately one order, which coincides with the results of Chan et al. (2001) and Baik et al. (1999).



Baik et al. (1999) simulated the flow field in urban street canyon with a different aspect ratio. They validated the simulation results with water a channel experiment conducted by Odell and Kovaszny (1971). Using the same method, this study compares the flow field with the water channel experiment results of Odell and Kovaszny (1971).

The vertical profile of the normalized vertical velocity at an upstream position ($x/W = 0.125$), a center position ($x/W = 0.5$) and a downstream position ($x/W = 0.875$) with $H/W = 1$ and $H/W = 2$ are shown in Figure 7 and the results were compared with the results of Baik et al. (1999). The comparison shows that the flow field is acceptable.

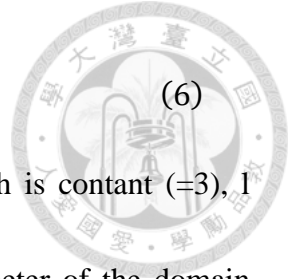
2.6.2 Evaporation cooling validation

The validation of 3D steady RNG k- ϵ model coupled with steady DPM in ANSYS FLUENT follows the procedure of the validation done by Montazeri et al. (2015). The validation is based on wind tunnel experiments by Sureshkumar et al. (2008). In the experiment, a hollow-cone nozzle spray was installed in the middle of the inlet of the wind tunnel, and 9 wet bulb temperature meters (WBT) and dry bulb temperature (DBT) meters are installed on the outlet of the wind tunnel.

The boundary conditions of k and ϵ inlet boundary are shown as follow:

$$k = (V_i \times I)^2 \quad (5)$$

$$\varepsilon = \frac{C_{\mu}^{0.75} k^{1.5}}{l}$$



, where I (=10%) is turbulence intensity, V_i is inlet velocity which is constant (=3), l (=0.07 D_H) is turbulence length scale and D_H is the hydraulic diameter of the domain which is equal to the width of the wind tunnel (=0.585 m). DBT and WBT of inlet air are 39.2°C and 18.7°C respectively. The characteristic of water droplet are: $T_w=35.2^\circ\text{C}$, $V_w=22.05$ m/s, $\dot{m}=12.5$ kg/min, $\bar{D}=369$ μm , $D_{\min}=74$ μm , $D_{\max}=518$ μm , spread parameter $n=3.67$, total number of streams is 300 and 20 diameters injected from each droplet stream. The half-cone angle ($\alpha/2$) is 18° and the radius of the spray nozzle is 2 mm.

The results of DBT and humidity ratio simulations are compared with wind tunnel experiment and are shown in Figure 8. Errors of DBT are all within 10% of measurement data and errors of humidity ratio are about 20%. The error may be caused from the assumption of the model or the experiment measurement.



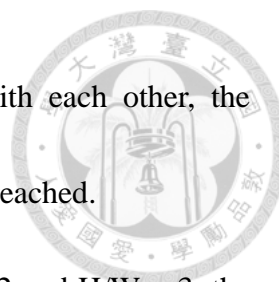
3. Results and discussion



3.1 Cooling effect with different aspect ratio and relative humidity

Figure 9 shows the velocity field in the street canyon before the spray nozzles operate with $H/W = 1, 2,$ and 3 (Cases 1.1, 2.1, and 3.1). There were two vortices in opposite direction in street canyon with $H/W = 2$ and $H/W = 3$ while there was only one vortex in street canyon with $H/W = 1$. Figure 10 shows the the same result as Figure 9 but after the spray nozzles operated. In the street canyon with $H/W = 2$ and $H/W = 3$, after the operation of spray systems, the lower vortex near ground (which was weaker than the upper one), vanished and formed the same pattern as that in the street canyon with $H/W = 1$. The wind velocity field near the ground was mainly affected by the spray nozzles rather than the wind flowing into street canyon from outside.

Figure 11 shows the temperature contours on the plane: $y = 0$ of Case 1.1 ($H/W = 1$), Case 2.1 ($H/W = 2$) and Case 3.1 ($H/W = 3$) at $t = 5$ sec. Figure 12 shows the same results but at steady state of Cases 1.1, 2.1, 3.1 ($RH = 70\%$), and 1.2, 2.2, 3.2 ($RH = 80\%$). After the spray nozzles started, the water droplets moved to the bottom due to large ($V_w = 15$ m/s) negative vertical velocity and higher density flow of cold air. Two puff of cold air cooled by the two groups of nozzles collapsed with each other in the middle of the street canyon. It took time for transient model to reach steady state (if

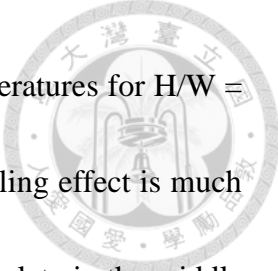


steady state exists). After the two puffs of cold air collapsed with each other, the contours only changed a little and steady state was considered to be reached.

The results show that in the street canyon with $H/W = 1$, $H/W = 2$ and $H/W = 3$, the cold air accumulated at the bottom although they had different flow fields in the street canyon. The patterns are similar for the same H/W with different RH as well. The temperature of cold air was lower in $RH = 70\%$ than that in $RH = 80\%$ (further discussion in section 3.3).

To see the cooling effect on plane: $y = 0$ at the average height of humans' chest or face ($z = 1.5$ m), the temperature profile on the line ($y = 0, z = 1.5$ m) with different aspect ratio and relative humidity in Case 1.1 ($H/W = 1, RH = 70\%$), Case 2.1 ($H/W = 2, RH = 70\%$), Case 3.1 ($H/W = 3, RH = 70\%$), Case 1.2 ($H/W = 1, RH = 80\%$), Case 2.2 ($H/W = 2, RH = 80\%$), Case 3.2 ($H/W = 3, RH = 80\%$) was plotted in Figure 13. Under the nozzles, the air temperature reduced rapidly in all the cases. However, in $H/W = 3$ ($W = 5$ m), the cold air accumulated in the middle of the street canyon, causing the most effective cooling effect among these cases.

The average temperatures on this line are 33.3 °C, 33.5 °C and 30.7 °C for Case 1.1, Case 2.1 and Case 3.1 respectively; the average temperature on this line are 34.0 °C, 34.0 °C and 32.1 °C for Case 1.2, Case 2.2 and Case 3.2 respectively (Table 4). When the



relative humidity decreased from 80% to 70%, the reduction of temperatures for $H/W = 1$, $H/W = 2$, $H/W = 3$ are $0.7\text{ }^{\circ}\text{C}$, 0.5°C , $1.4\text{ }^{\circ}\text{C}$ respectively. The cooling effect is much more sensitive for the cases with $H/W = 3$ because the cold air accumulate in the middle of the street canyon.

To check the influence range of the cooling effect along the y-direction, we drew the dispersion of cold air in x-y plane at $z = 1.5\text{ m}$ in Case 2.1. (Figure 12) At this height, the cold air spread in y direction at a very slow speed, the range of influence in the y direction is about 1 time of street width ($y < \pm 5\text{ m}$).

3.2 Effects of particle size and relative humidity

Figure 15 shows the temperature contour on the plane: $y = 0$ in Case 2.1 (small particle, $\bar{D} = 20\text{ }\mu\text{m}$, $V_w = 15\text{ m/s}$, $\dot{m} = 0.01\text{ kg/s}$) and Case 2.1a (large particle, $\bar{D} = 369\mu\text{m}$, $V_w = 22\text{m/s}$, $\dot{m} = 0.2\text{ kg/s}$) respectively. In Case 2.1, the cold air is almost around $30\text{ }^{\circ}\text{C}$, while in Case 2.1a, the cold air is around 32° C , instead. However, most of the cold air of Case 2.1 accumulated at the bottom. In Case 2.1a, because of the large velocity of wind cause by the nozzles, the cold air can spread out more than in Case 2.1. Figure 16 shows the horizontal temperature profile in x-direction at $y = 0$ and $z = 1.5\text{ m}$ (which is the average height of humans' chest and face) of these two cases. The average

temperatures for Case 2.1 and Case 2.1a are 33.5 °C and 32.2 °C respectively, showing that Case 2.1a (large particle) has better cooling effect at the height = 1.5 m.



Figure 17 shows the time that particles reach the ground (residence time) of the particles in these two cases. The residence time are about 2 seconds for Case 2.1 and about 0.7 seconds for Case 2.1a. Case 2.1a has the shortest residence time because the particle of Case 2.1a is much bigger and the velocity is much higher.

Figure 18 shows the temperature contours on the plane: $y = 0$ in Case 2.1 (RH = 70%), Case 2.2 (RH = 80%). After leaving the nozzles, the air quickly reached a fixed temperature (30 °C for RH = 70%, 32°C for RH = 80%). Figure 19 shows the RH contour in Case 2.1 (RH = 70%, $\bar{D} = 20 \mu\text{m}$), Case 2.2 (RH = 80%, $\bar{D}=20 \mu\text{m}$), Case 2.1a (RH = 70%, $\bar{D}= 369 \mu\text{m}$) and Case 2.2a (RH = 80%, $\bar{D} = 369 \mu\text{m}$). If the water vapour is saturated, evaporation of the droplet stops and the temperature reaches a lower bound, which is near the wet bulb temperature (the wet-bulb temperature with specific air temperature and humidity is listed in appendix A.2). If saturation occurs, increasing the residence time or mass flow rate of water has no effect, as we can see in Figure 19 (a) and (b). If saturation has not occurred yet, the air will not reach the lowest temperature as we can see in Figure 19 (c) and (d). For the cases with $\bar{D} = 369 \mu\text{m}$ and

RH = 70%, residence time is too small to saturate the air. However, when the RH is 80%, the saturation will be easily achieved.



3.3 Effects of height of spray nozzles

One way to increase residence time in order to saturate the air is to increase the height of the spray nozzles. Figure 20 shows the horizontal temperature profile in x-direction at $y = 0$ and $z = 1.5$ m in Case 2.1a ($h_s = 2.5$ m), Case 2.1b ($h_s = 3$ m) and Case 2.1c ($h_s = 3.5$ m). In increasing the nozzles height from 2.5 m to 3.5 m, the air just under the nozzles at height = 1.5 m became totally saturated. However, the temperature and humidity differences among these cases at height = 1.5 m were not significant because the air was almost saturated at this height. As a result, when RH = 70%, all the nozzles can almost saturate the air before droplets fall below 1.5 m. This indicates that increasing the nozzle heights would not increase the cooling effect.

4. Conclusions

This study simulates the cooling effect of water spray systems in the urban street canyon using the Computational Fluid Dynamics (CFD) method; and the 3D unsteady k- ϵ model coupled with discrete phase model (DPM) provided by ANSYS FLUENT

was adopted. The model validation was carried out by flow fields of the urban street canyon measured in water channel experiments.

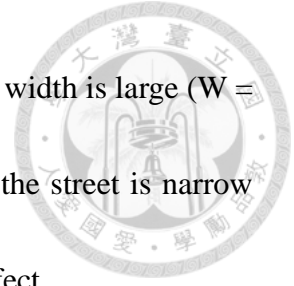


The results showed that after the droplets were injected, they dropped directly to the ground even the mean droplet size was very small (20 μm); this was due to the wind velocity in the street canyon being very weak. In a narrow street canyon ($H/W = 3$), cold air would accumulate in the street, causing the best cooling to happen at a height 1.5 m (which is the average height of humans' chest and face) when spray nozzles were set at the height of 2.5 m.

For all the cases with 35 $^{\circ}\text{C}$ air temperature and $\text{RH} > 70\%$, which is often the case in summers in Taipei, both large and small water droplets can almost saturate the air just under the nozzles at 1.5 m height, so the lowest temperature is achieved. The lowest temperatures for $\text{RH} = 70\%$ and 80% were around 30 $^{\circ}\text{C}$ and 32 $^{\circ}\text{C}$, respectively, which were near the wet bulb temperatures of these two cases. In addition, the cooling effect for cases with $H/W = 3$ was much more sensitive to the relative humidity change than those in the other two aspect ratios, because the cold air accumulated in the middle of the narrow street canyon.

In summary, for the typical summer weather conditions in Taipei city, the height of nozzle and particle size were not the determinant parameters because the lowest

temperature (wet bulb temperature) was easily achieved. If the street width is large ($W = 15$ m, $W = 10$ m), the coolest position is just under the nozzles. If the street is narrow ($W = 5$ m), people in the middle of the street may feel the cooling effect.



Appendix



A.1 Governing equations of continuous phase

The continuous phase model is solved based on mass, momentum, energy conservation principle. Reynolds average method which consider the transport of mean velocity (U_i), turbulence kinetic energy (k) and kinetic energy dissipation rate (ϵ) is used to solve the turbulence flow. In this study, the Renormalized Group (RNG) k - ϵ was used. The government equations are:

(1) The mass conservation equation (for incompressible flow):

$$\frac{\partial(\rho U_i)}{\partial x_j} = S_m. \quad (\text{A.1})$$

S_m is the source term of mass that added to continuous phase because of the evaporation of water ($\text{kg}/\text{m}^3\text{s}$).

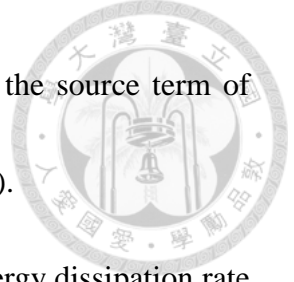
(2) The momentum conservation equation:

$$\frac{\partial U_i}{\partial t} + U_j \frac{\partial U_i}{\partial x_j} = -\frac{1}{\rho} \frac{\partial P}{\partial x_i} + \nu \frac{\partial^2 U_i}{\partial x_j^2} - \frac{\partial \overline{u_i' u_j'}}{\partial x_j} + g_i + \frac{F_i}{\rho}, \quad (\text{A.2})$$

$$\overline{u_i' u_j'} = \frac{2}{3} \delta_{ij} k - \nu_t \left(\frac{\partial U_i}{\partial x_j} + \frac{\partial U_j}{\partial x_i} \right), \quad (\text{A.3})$$

$$\nu_t = C_\mu \frac{k^2}{\epsilon}, \quad (\text{A.4})$$

where u_i' is the velocity fluctuation in i direction (m/s), ν is molecular kinematic viscosity (m^2/s), g is gravity acceleration (m/s^2), ν_t is turbulent kinematic viscosity



(m²/s), C_μ is a constant which is 0.0845 in RNG k- ϵ model, F_i is the source term of force in i direction exerted on continuous phase by discrete phase (N).

(3) The conservation of turbulence kinetic energy (k) and kinetic energy dissipation rate

(ϵ):

$$\frac{\partial k}{\partial t} + U_j \frac{\partial k}{\partial x_j} = \frac{\partial}{\partial x_j} \left[\alpha_k \frac{\partial k}{\partial x_j} \right] + G_b + G_k - \epsilon, \quad (\text{A.5})$$

$$\frac{\partial \epsilon}{\partial t} + U_j \frac{\partial \epsilon}{\partial x_j} = \frac{\partial}{\partial x_j} \left[\alpha_k \nu_{eff} \frac{\partial \epsilon}{\partial x_j} \right] + \frac{1}{\rho} C_{1\epsilon} \frac{\epsilon}{k} (C_{3\epsilon} G_b + G_k) - C_{2\epsilon}^* \frac{\epsilon^2}{k}, \quad (\text{A.6})$$

here,

$$C_{1\epsilon} = 1.42,$$

ν_{eff} is effective turbulent kinematic viscosity ($\nu_{eff} = \nu + \nu_t$),

$$G_b = \rho \beta g \frac{\nu_t}{Pr_t} \frac{\partial T}{\partial x_i},$$

$$G_k = \nu_t \times \frac{\partial U_i}{\partial x_j} \left(\frac{\partial U_i}{\partial x_j} + \frac{\partial U_j}{\partial x_i} \right),$$

β is the thermal expansion coefficient in the form:

$$\beta = \frac{1}{\rho} \left(\frac{\partial \rho}{\partial T} \right)_p,$$

$$C_{2\epsilon}^* = C_{2\epsilon} + \frac{C_\mu \rho \eta^3 \left(1 - \frac{\eta}{\eta_0} \right)}{1 + a\eta^3},$$

$\eta = Sk/\epsilon$, S is the scalar measure of the deformation tensor, η_0 and a are 4.38 and 0.012

respectly, $C_{2\epsilon} = 1.68$.

α_k and α_ϵ are the inverse effective Prantl numbers and are computed as follow by the

RNG theory:



$$\left| \frac{\alpha - 1.3929}{\alpha_0 - 1.3929} \right|^{0.6321} \left| \frac{\alpha + 2.3929}{\alpha_0 + 2.3929} \right|^{0.3679} = \frac{\nu}{\nu_{eff}},$$

$\alpha_0 = 1.0$. in high-Reynolds number limit, $\alpha_k = \alpha_\epsilon \approx 1.393$.

$$C_{3\epsilon} = \tanh \left| \frac{W}{\sqrt{U^2 + V^2}} \right|.$$

(4) Water vapour mass conservation:

$$\frac{\partial C}{\partial t} + U_i \frac{\partial C}{\partial x_i} = D_m \frac{\partial^2 C}{\partial x_i^2} + \frac{\partial}{\partial x_i} \left(D_t \frac{\partial C}{\partial x_i} \right) + S_v. \quad (\text{A.7})$$

,where D_m is molecular diffusivity (m^2/s), D_t is turbulent diffusivity (m^2/s), which can be obtained by $Sc_t = \frac{\nu_t}{D_t}$, where Sc_t is the turbulent Schmidt number. In RNG k- ϵ model,

$Sc_t = 0.7$. S_v is the source term due to the evaporation of the droplet in discrete particle model.

(5) Energy conservation equation:

$$\frac{\partial}{\partial t} (\rho E) + \frac{\partial}{\partial x_i} [u_i (\rho E + p)] = \frac{\partial}{\partial x_j} \left(k + \frac{c_p \mu_t}{Pr_t} \right) + S_h \quad (\text{A.8})$$

where Pr_t (turbulent Prandtl number) is 0.85 for k- ϵ model, S_h is source term which is contributed by latent heat absorbed during the evaporation of droplets. E is total energy of the fluid ($\text{J}/\text{kg}/\text{m}^3$):

$$E = \int_{T_{ref}}^T C_p dT + \frac{v^2}{2}.$$



A.2 Governing equations of discrete phase (water droplets)

(1) Particle force balance:

$$\frac{d\vec{u}_p}{dt} = \frac{18\mu}{\rho_p d_p^2} \frac{C_D Re}{24} (\vec{u} - \vec{u}_p) + \frac{\vec{g}(\rho_p - \rho)}{\rho_p}, \quad (\text{A.9})$$

, where \vec{u}_p is the particle velocity (m/s), \vec{u} is the air velocity (m/s), μ is the molecular viscosity of the air (kg/m/s), ρ_p is the density of particle (kg/m³), d_p is the diameter of particle (m), C_D is the drag coefficient, ρ is the density of air (kg/m³), \vec{g} is gravity acceleration (m/s²), Re is the droplet Reynolds number, which is defined as $Re = \frac{\rho d_p |\vec{u}_p - \vec{u}|}{\mu}$.

Here, the water droplets are assume to be sphere particles, and the drag coefficient of sphere particles is as follows:

$$C_D = a_1 + \frac{a_2}{Re} + \frac{a_3}{Re^2} \quad (\text{A.10})$$

, where a_1 , a_2 and a_3 are constants given with different ranges of Re (Morsi and Alexander, 1972).

(2) Particle mass transfer:

The water droplets evaporate and transfer the mass into the air. The water droplets are modeled as particles surrounded by saturated air-vapor films, when the concentration of water vapor in the films larger than that in the air, the gradient cause the water vapor diffuse from the film to the air.

The mass transfer rate is as follow:

$$\frac{dm_p}{dt} = M_p A_p k_c (C_s - C_a) \quad (\text{A.11})$$

, where m_a is the mass of the particle (kg), M_p is the molecular weight of the particle (kg/mol), A_p is the surface area of the particle (m²), k_c is the mass transfer

coefficient (m/s), C_s is the vapor concentration at the surface (saturated air-vapor film) (mol/m^3), which is calculated by: $C_s = p_{sat}/RT_p$, where p_{sat} is the saturated vapor pressure at the particle temperature (T_p), R is the universal gas constant, C_a is the vapor concentration in the air (mol/m^3).

k_c was calculated from the empirical correlation of Sherwood number (Ranz and Marshall, 1952):

$$\text{Sh} = \frac{k_c d_p}{D} = 2 + 0.6 \cdot Re^{0.5} \cdot Sc^{0.33} \quad (\text{A.12})$$

,where Sh is the Sherwood number, D is the diffusion coefficient of vapor (m^2/s), Sc is the Schmidt number, which is given as: $Sc = \mu/\rho D$.

(3) Particle heat transfer:

$$m_p C_{pw} \frac{dT_p}{dt} = h A_p (T_a - T_p) - \frac{dm_p}{dt} \frac{\lambda}{M_p} \quad (\text{A.13})$$

,where C_{pw} is the specific heat of water droplet (J/kg), λ is the latent heat of water (44kJ/mol), h is the convection heat transfer coefficient, which was calculated from the empirical correlation of Nu number when vapor mass fraction $\ll 1$ (Sazhin, 2006):

$$\text{Nu} = \frac{hd_p}{k_a} = 2 + 0.6 Re^{0.5} Pr^{0.33} \quad (\text{A.14})$$

,where k_a is the thermal conductivity of the continuous phase, Pr is the Prandtl number of the continuous phase, which is given as: $Pr = c_p \mu/k_a$.



A.3 The derivation of wet bulb temperature

The wet-bulb temperature is the temperature that an air parcel would reach when it was cooled and saturated by the evaporation of water. And the wet-bulb temperature can be determined by (Campell and Norman, 2012):

$$(T_a - T_w)C_p = [(e_s(T_w) - e_a)/P_a]\lambda \quad (\text{A.15})$$

,where T_a is the air temperature (K), T_w is wet bulb temperature (K), C_p is the specific heat of air (29.3 J/mol/K), $e_s(T_w)$ is the saturate vapour pressure at T_w (Pa), e_a is the initial vapour pressure at T_a (Pa), P_a is air pressure (Pa), λ is the latent heat of water (44kJ/mol). $e_s(T_w)$ is calculated by: $e_s = 611 \cdot \exp\left(\frac{17.27 \cdot T'_w}{T'_w + 237.3}\right)$, where T'_w is T_w expressed in Celsius.

Hence, equation (A.15) provides an analytical solution for the lowest temperature which the cooling effect can reach by the water spray system.



A.4 Extra cases

A.4.1 Nozzles set on one side (left side or right side) of the street

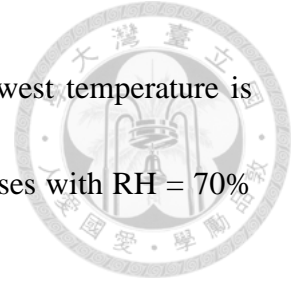
The spray nozzles in the cases in Table 2 were set on both side (left and right) of the street. However, in often cases the nozzles are only set on one side of the street. To compare the cooling effect of the cases that the nozzles are only set on one side, extra 4 cases with nozzles were set on the left side or on the right side in the street with $H/W = 1$ and $H/W = 2$ were done and the temperature contour were shown in Figure 21.

In the cases with $H/W = 1$, the wind velocity was large enough to blow the water droplets away, so the cold air in the windward side (the right side in our cases) would spread out to the other side but the cold air in the leeward side (the left side in our cases) would accumulate. However, in the cases with $H/W = 2$, the wind velocity was too small to blow the water droplet away, so the cooling effect of both cases were similar. The temperature profile at $z = 1.5$ m were shown in Figure 22.

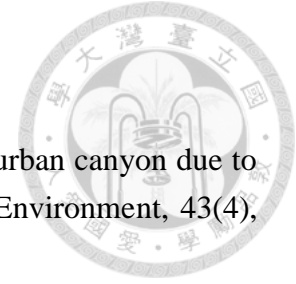
A.4.2 RH = 60%

The relative humidity in summer in Taiwan often reach 60% as well. To see the cooling effect when $RH = 60\%$, extra cases with $H/W = 1, 2$ and 3 were done. The temperature contours were shown inFigure 23. The patterns of the cooling effect were

similar with the cases with $RH = 70\%$ and 80% . However, the lowest temperature is about 28°C in the cases with $RH = 60\%$, which is lower than the cases with $RH = 70\%$ and 80% .



Reference



Alexandri, E., & Jones, P. (2008). Temperature decreases in an urban canyon due to green walls and green roofs in diverse climates. *Building and Environment*, 43(4), 480-493.

ANSYS Inc. (2013). ANSYS fluent 15.0 theory guide.

Baik, J. J., & Kim, J. J. (1999). A numerical study of flow and pollutant dispersion characteristics in urban street canyons. *Journal of applied meteorology*, 38(11), 1576-1589.

Baik, J. J., Park, R. S., Chun, H. Y., & Kim, J. J. (2000). A laboratory model of urban street-canyon flows. *Journal of applied meteorology*, 39(9), 1592-1600.

Campbell, G. S., & Norman, J. M. (2012). An introduction to environmental biophysics. Springer Science & Business Media. Chapter 3, page 44.

Chan, T. L., Dong, G., Leung, C. W., Cheung, C. S., & Hung, W. T. (2002). Validation of a two-dimensional pollutant dispersion model in an isolated street canyon. *Atmospheric environment*, 36(5), 861-872.

Huang, C., Ye, D., Zhao, H., Liang, T., Lin, Z., Yin, H., & Yang, Y. (2011). The research and application of spray cooling technology in Shanghai Expo. *Applied Thermal Engineering*, 31(17), 3726-3735.

Isaac, M., & Van Vuuren, D. P. (2009). Modeling global residential sector energy demand for heating and air conditioning in the context of climate change. *Energy policy*, 37(2), 507-521.

Jain, S. P., & Rao, K. R. (1974). Experimental study on the effect of roof spray cooling on unconditioned and conditioned buildings. *Building Science*, 9(1), 9-16.

Kang, D., & Strand, R. K. (2013). Modeling of simultaneous heat and mass transfer within passive down-draft evaporative cooling (PDEC) towers with spray in FLUENT. *Energy and Buildings*, 62, 196-209.

Launder, B. E., & Spalding, D. B. (1974). The numerical computation of turbulent flows. *Computer methods in applied mechanics and engineering*, 3(2), 269-289.

Montazeri, H., Blocken, B., & Hensen, J. L. M. (2015). Evaporative cooling by water spray systems: CFD simulation, experimental validation and sensitivity analysis. *Building and environment*, 83, 129-141.

Montazeri, H., Toparlak, Y., Blocken, B., & Hensen, J. L. M. (2017). Simulating the cooling effects of water spray systems in urban landscapes: A computational fluid dynamics study in Rotterdam, The Netherlands. *Landscape and Urban Planning*, 159, 85-100.

Morsi, S., & Alexander, A. J. (1972). An investigation of particle trajectories in two-phase flow systems. *Journal of Fluid Mechanics*, 55(2), 193-208.

Odell, G. M., & Kovaszny, L. S. (1971). A new type of water channel with density stratification. *Journal of Fluid Mechanics*, 50(03), 535-543.

Ranz, W. E., & Marshall, W. R. (1952). Evaporation from drops. *Chem. Eng. Prog*, 48(3), 141-146.

Runsheng, T., Etzion, Y., & Erell, E. (2003). Experimental studies on a novel roof pond configuration for the cooling of buildings. *Renewable Energy*, 28(10), 1513-1522.

Sarrat, C., Lemonsu, A., Masson, V., & Guedalia, D. (2006). Impact of urban heat island on regional atmospheric pollution. *Atmospheric environment*, 40(10), 1743-1758.

Sazhin, S. S. (2006). Advanced models of fuel droplet heating and evaporation. *Progress in energy and combustion science*, 32(2), 162-214.

Sureshkumar, R., Kale, S. R., & Dhar, P. L. (2008). Heat and mass transfer processes between a water spray and ambient air—I. Experimental data. *Applied Thermal Engineering*, 28(5), 349-360.



Table

Table 1 Summary of parameters in the CFD model

Roughness of no-slip boundary		Particle size distribution (Rosin-Rammler)		Characteristic of spray			
k_s	C_s	n	Number of diameters	$\alpha/2$	Points of injection	radius	T_w
1.5	0.5	3.5	10	20°	15	2 mm	25 °C

Time step size		Time step per injection
Continuous phase time step	Particle time step	0.05 sec
0.05 sec	0.001 sec	

k_s is the roughness height of the buildings and street, C_s is the roughness constant of the buildings and street, n is the spread parameter of the nozzles, $\alpha/2$ is the half cone angle of the nozzles, T_w is water temperature.

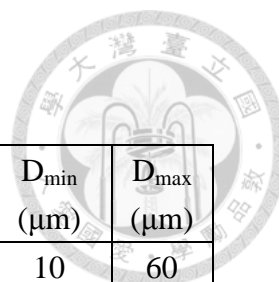


Table 2 List of the parameters of the Cases

Group	Case	H/W	RH (%)	h_s (m)	V_w (m/s)	\dot{m} (kg/s)	\bar{D} (μm)	D_{\min} (μm)	D_{\max} (μm)
1	1.1	1	70	2.5	15	0.01	20	10	60
	1.2	1	80	2.5	15	0.01	20	10	60
2	2.1	2	70	2.5	15	0.01	20	10	60
	2.1a	2	70	2.5	22	0.2	369	74	518
	2.1b	2	70	3	22	0.2	369	74	518
	2.1c	2	70	3.5	22	0.2	369	74	518
	2.2	2	80	2.5	15	0.01	20	10	60
	2.2a	2	80	2.5	22	0.2	369	74	518
3	3.1	3	70	2.5	15	0.01	20	10	60
	3.2	3	80	2.5	15	0.01	20	10	60

H/W is the aspect ratio of street canyon, RH (%) is relative humidity, V_w (m/s) is the velocity of water droplet, \dot{m} (kg/s) is water mass flow rate, \bar{D} (μm) is the mean particle size of water droplet, D_{\min} (μm) is the smallest particle size of water droplet, D_{\max} (μm) is the largest particle size of water droplet.

Table 3 The linear regression and root mean square error (RMSE) between experiment, the simulation results of Baik et al. (1999) and our predict results .

H/W = 1			
	linear regression	R ²	RMSE
Baik	$y=0.794 x - 0.0153$	0.9645	1.06
predict	$y=1.126 x - 0.0068$	0.9524	1.51
H/W = 2			
	linear regression	R ²	RMSE
Baik	$y=0.765 x - 0.0024$	0.7678	0.55
predict	$y=0.860 x + 0.0023$	0.6699	0.66

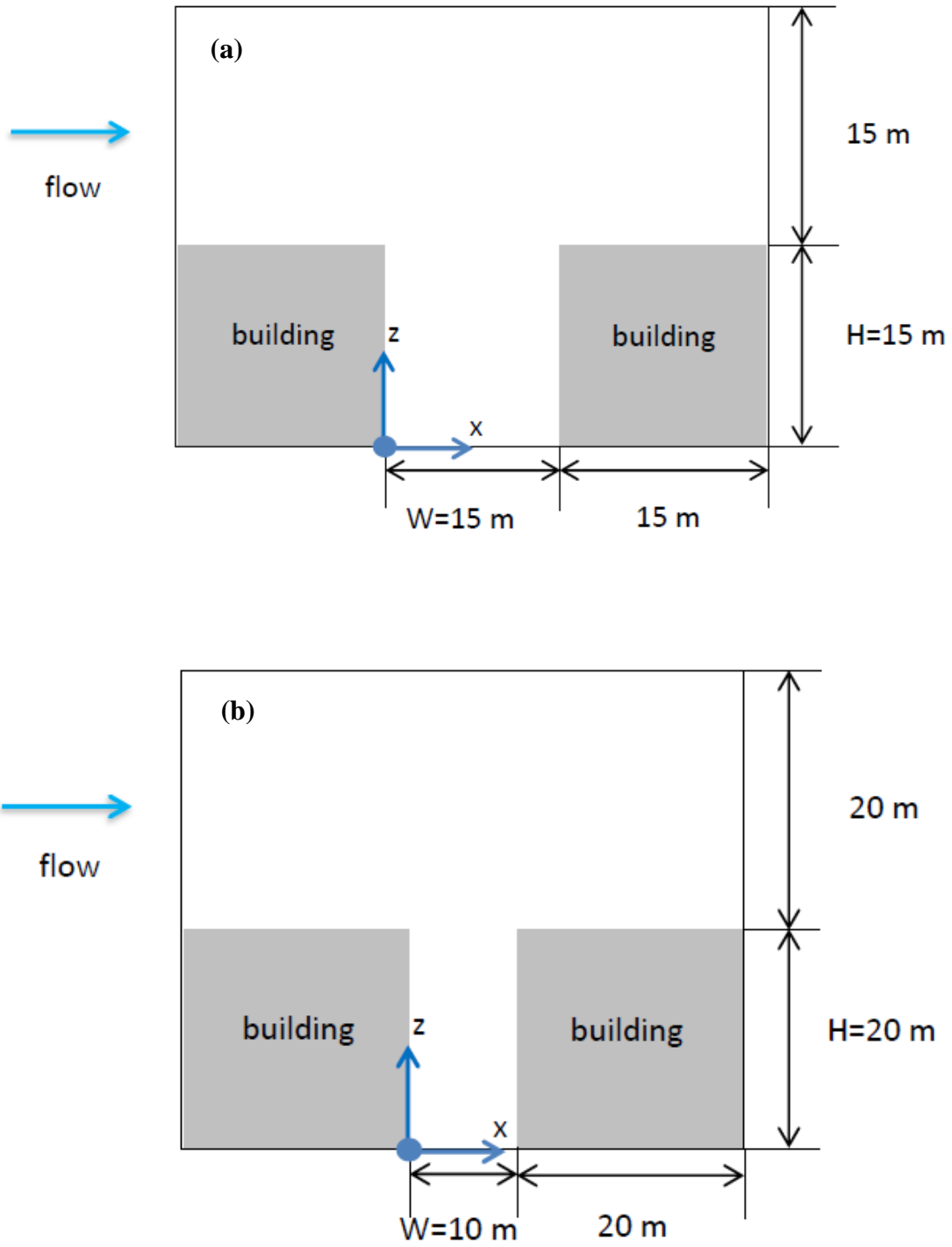
‘x’ in linear regression were experiment datas.

Table 4 Average temperature on the line: $y = 0$, $z = 1.5$ m with different aspect ratio and relative humidity in Case 1.1 ($H/W = 1$, $RH = 70\%$), Case 2.1 ($H/W = 2$, $RH = 70\%$), Case 3.1 ($H/W = 3$, $RH = 70\%$), Case 1.2 ($H/W = 1$, $RH = 80\%$), Case 2.2 ($H/W = 2$, $RH = 80\%$), Case 3.2 ($H/W = 3$, $RH = 80\%$). The background temperature is 35 °C.

	RH = 70%	RH = 80%	Reduction of temperature
H/W = 1	33.3 °C	34.0 °C	0.7 °C
H/W = 2	33.5 °C	34.0 °C	0.5 °C
H/W = 3	30.7 °C	32.1 °C	1.4 °C



Figure



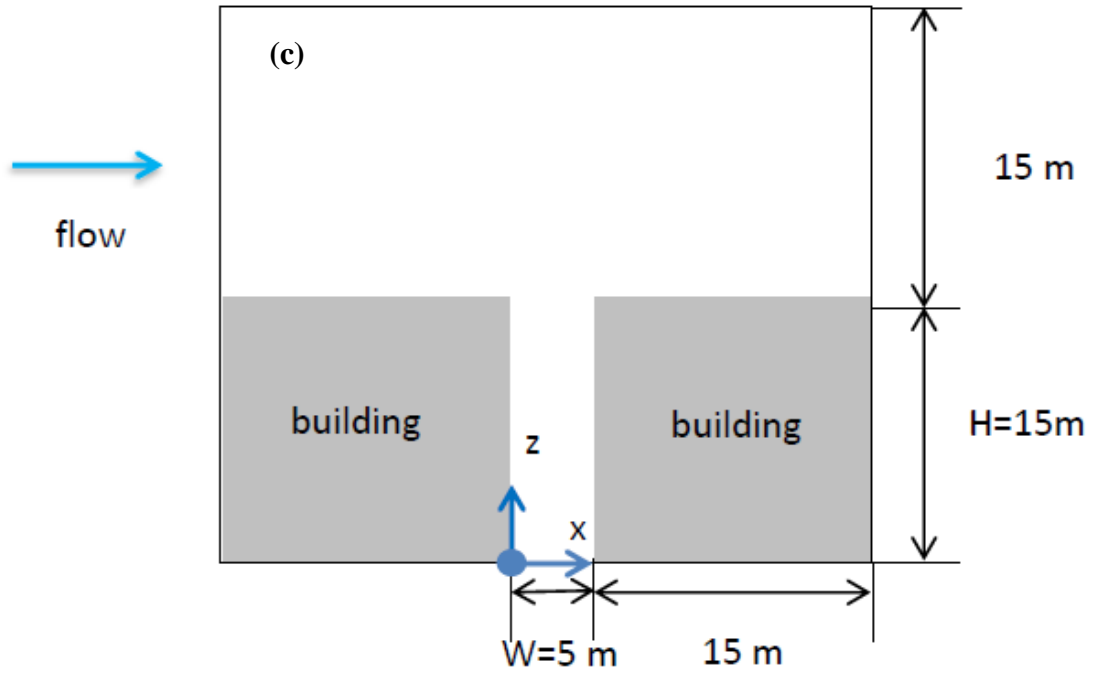
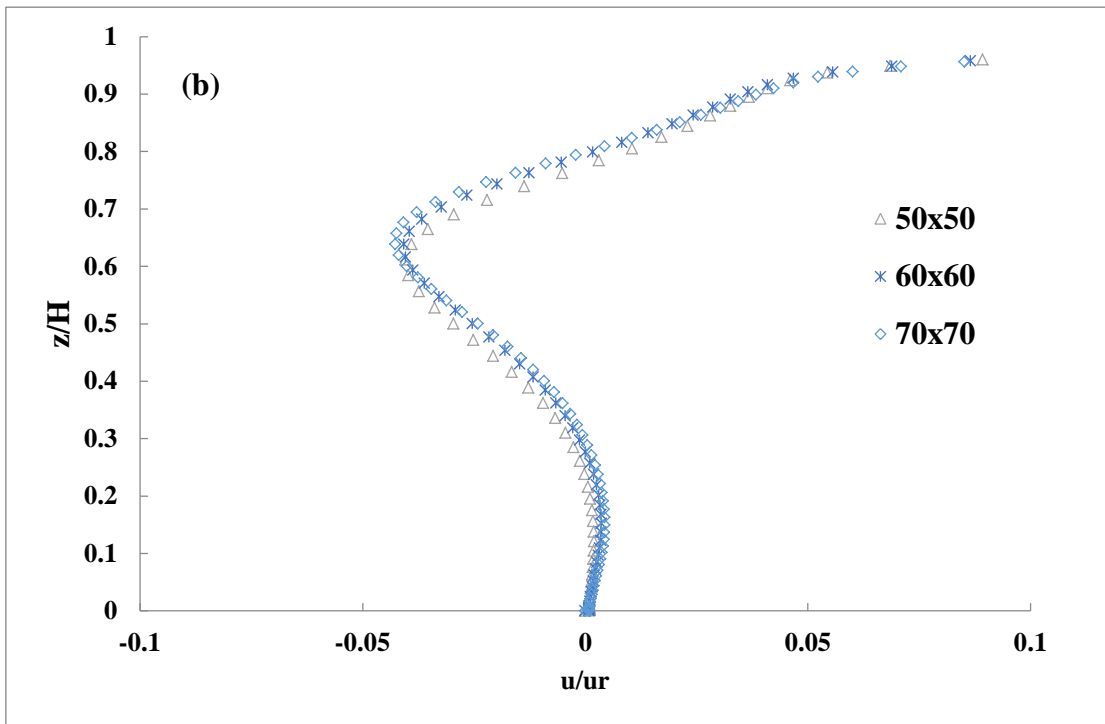
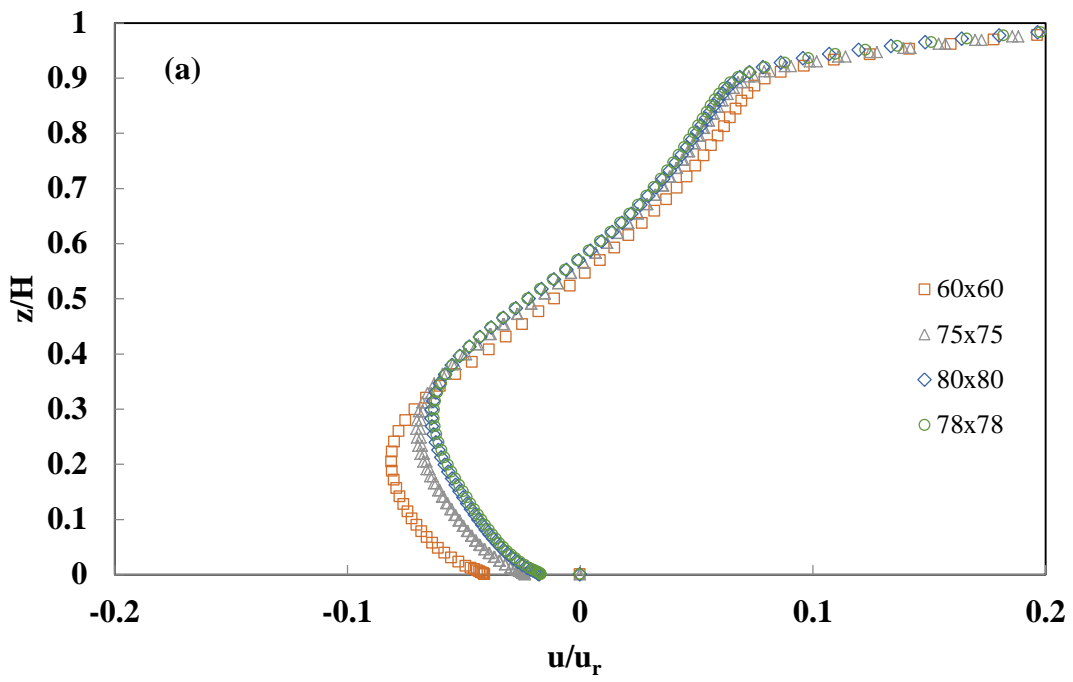


Figure 1 Computational domain for a street canyon. (a) $H/W = 1$. (b) $H/W = 2$. (c) $H/W = 3$.



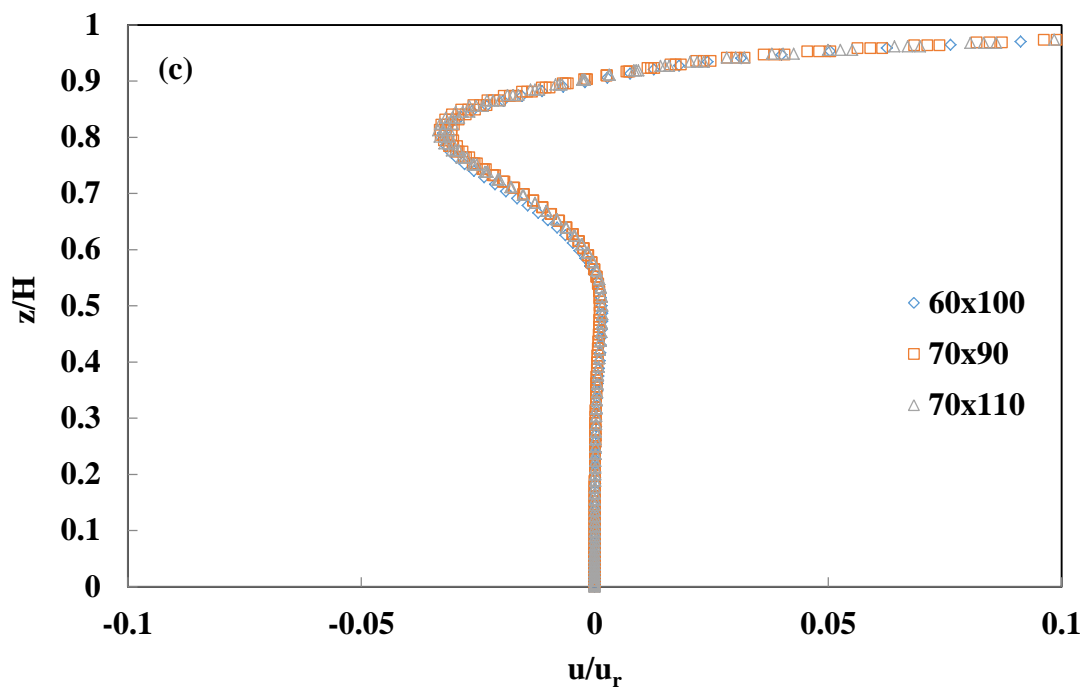
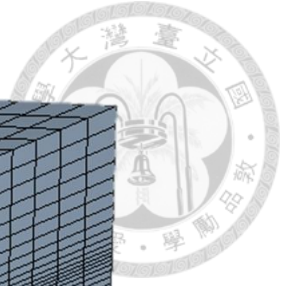
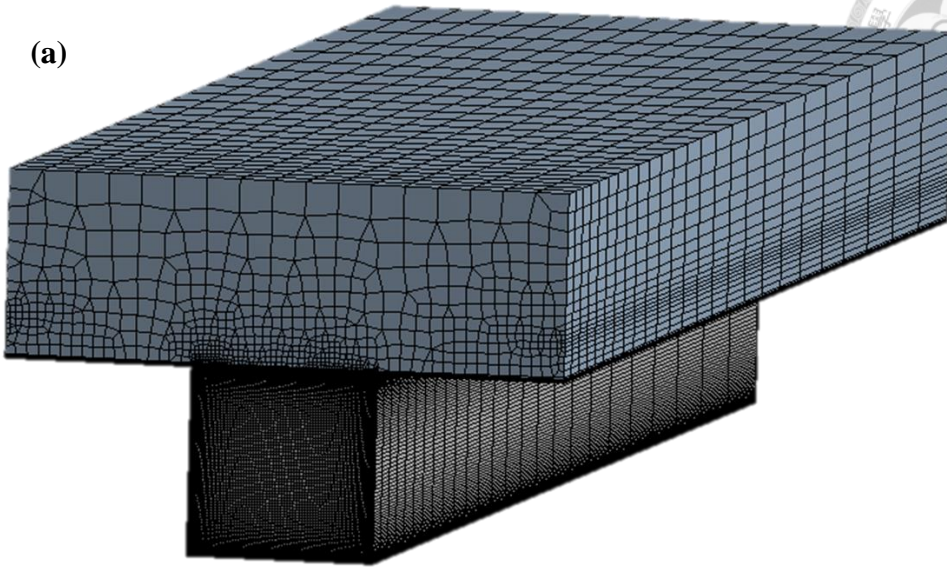


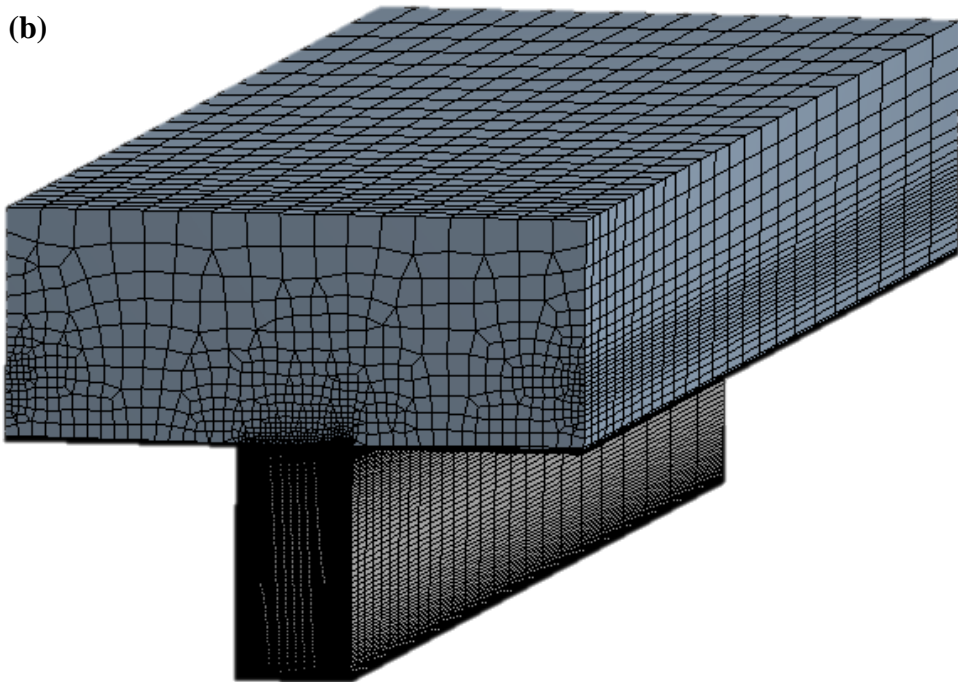
Figure 2 The vertical profile of the normalized horizontal velocity (u) at $x/W = 0.5$ and $y = 0$ for different mesh sizes in the urban street canyon. u_r is reference velocity which is set to be 4 m/s. (a) $H/W = 1$. (b) $H/W = 2$. (c) $H/W = 3$.



(a)



(b)



(c)

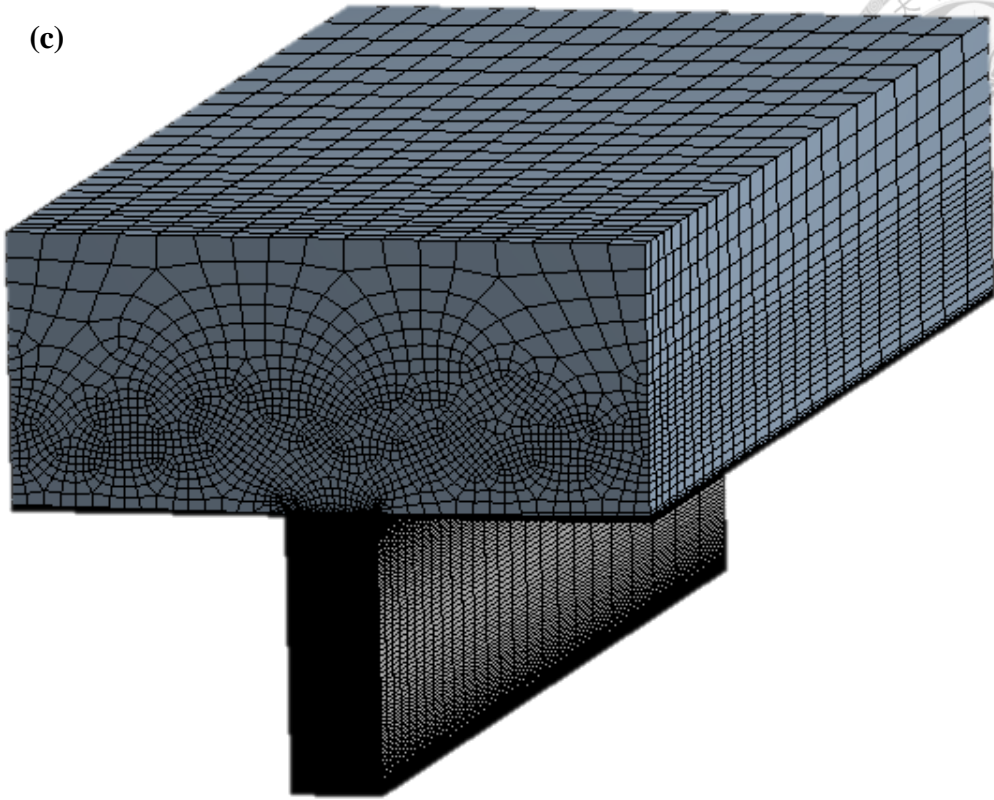


Figure 3 Computational domain and meshing. (a) $H/W = 1$. (b) $H/W = 2$. (c) $H/W = 3$.

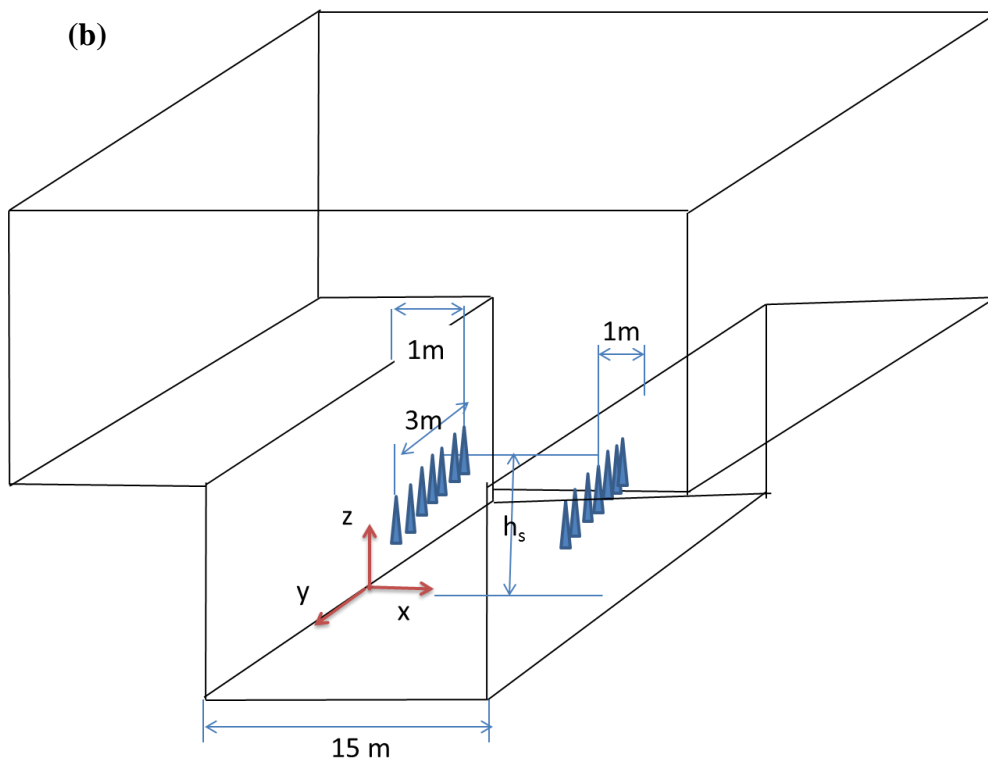
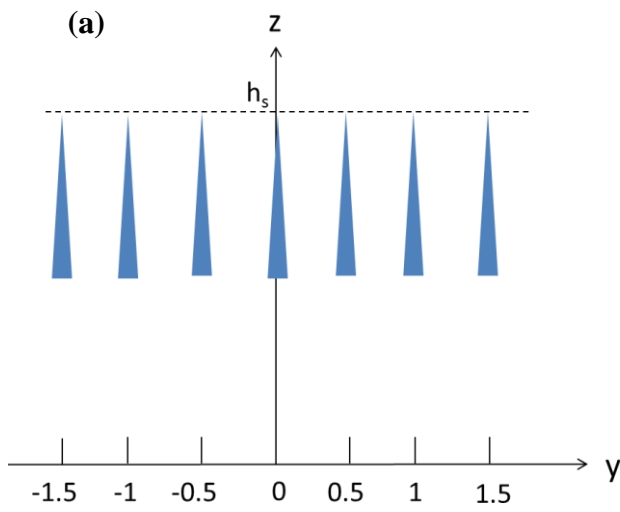
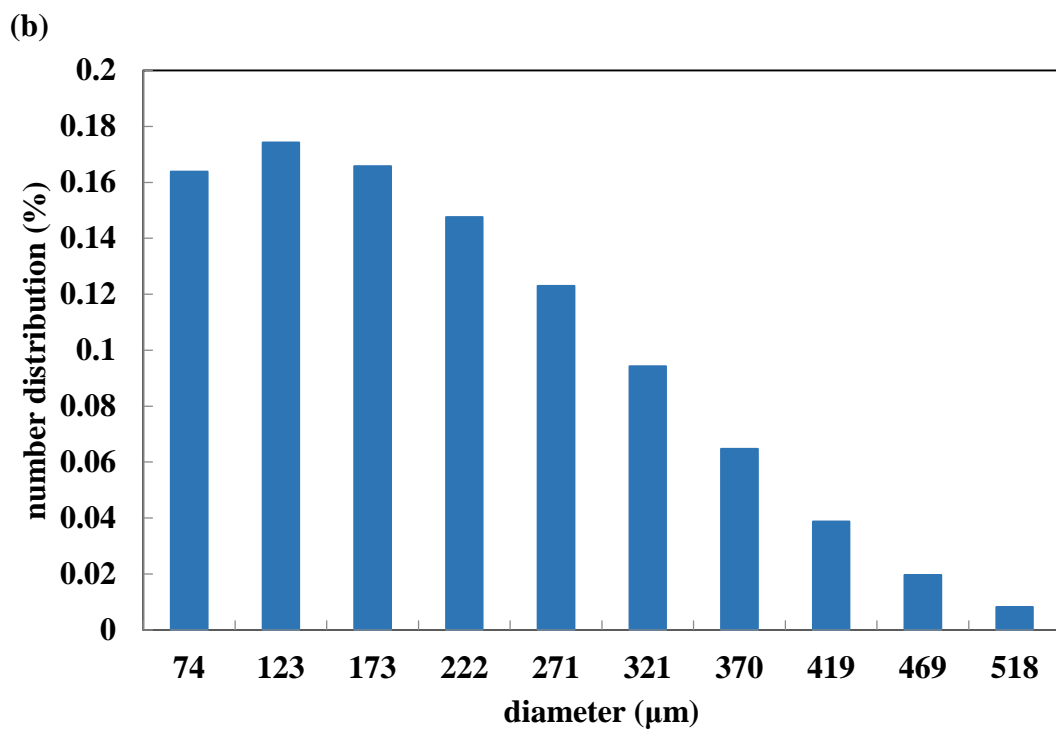
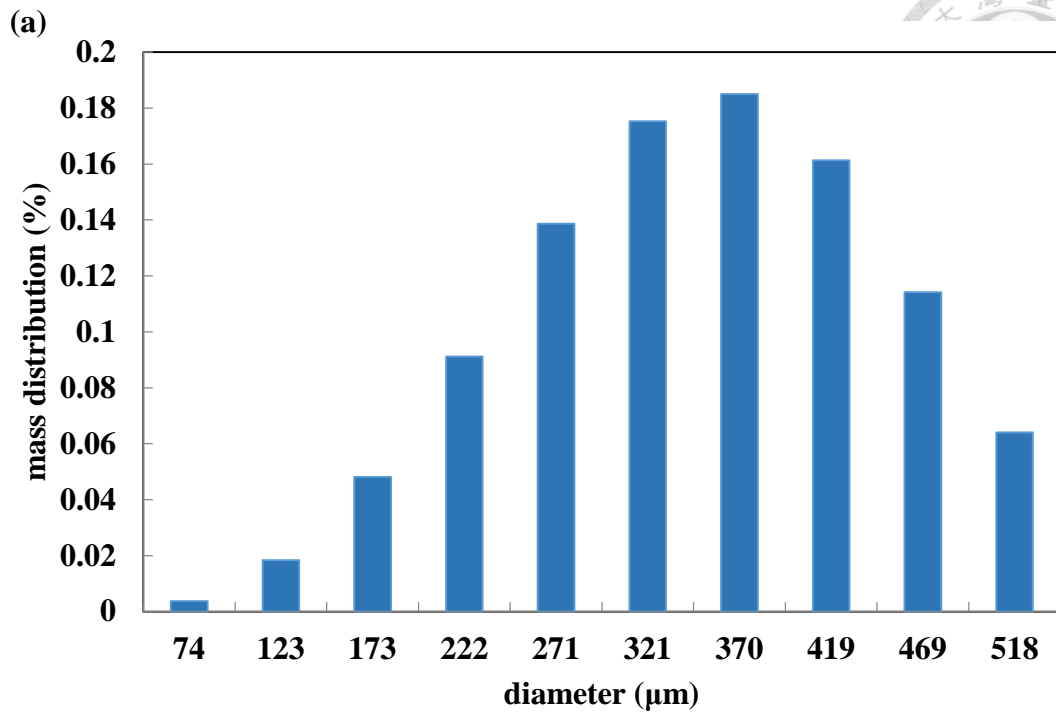


Figure 4 (a) View of a group of spray nozzles. (b) View of the urban street canyon with spray systems set in position $(x, z) = (1, 2.5)$ and $(x, z) = (14, 2.5)$. The y position of the spray nozzle are $\pm 1.5, \pm 1, \pm 0.5, 0$.



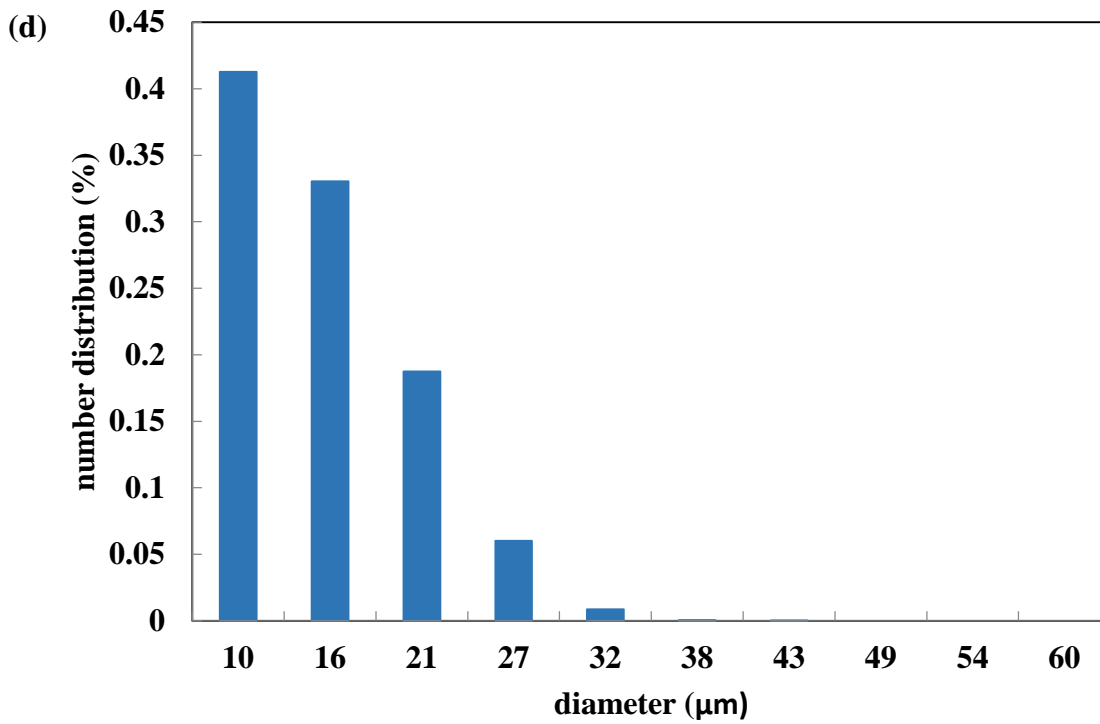
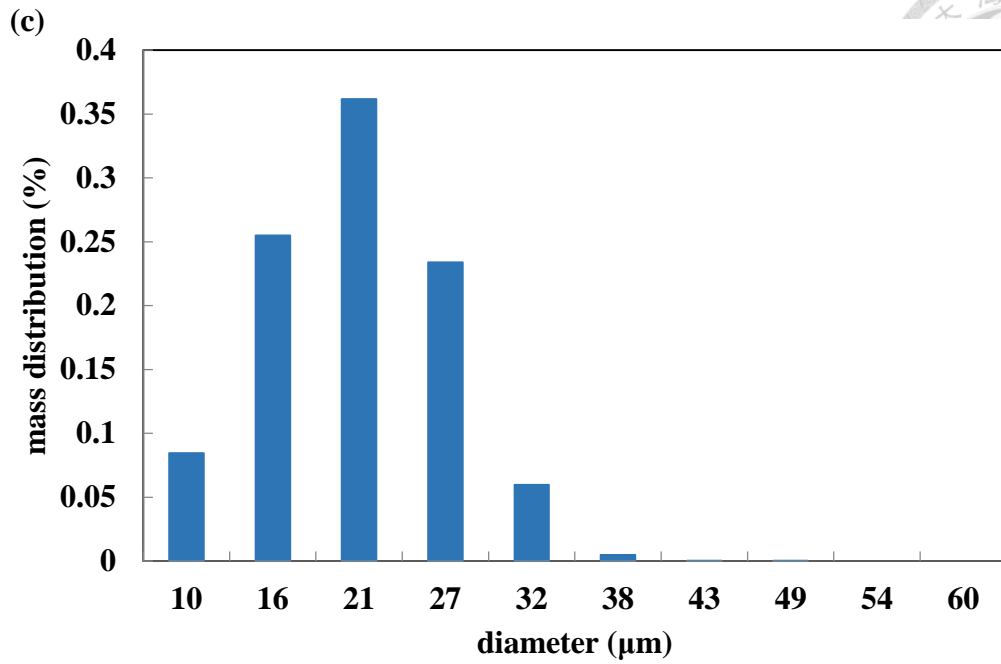
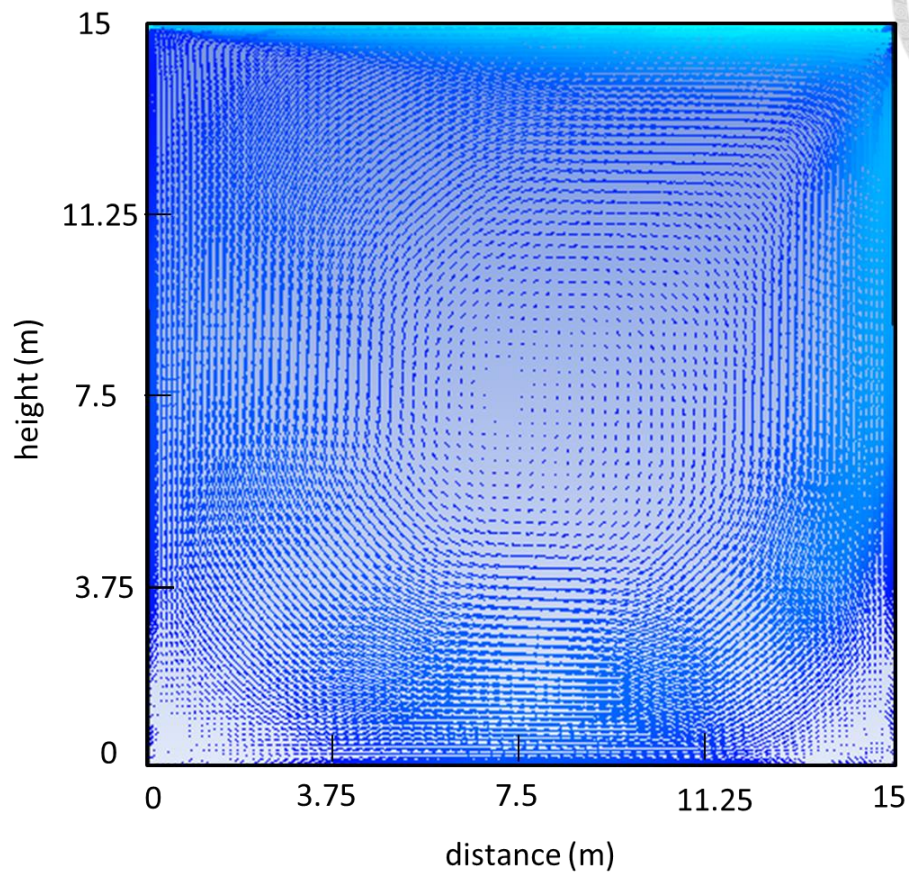
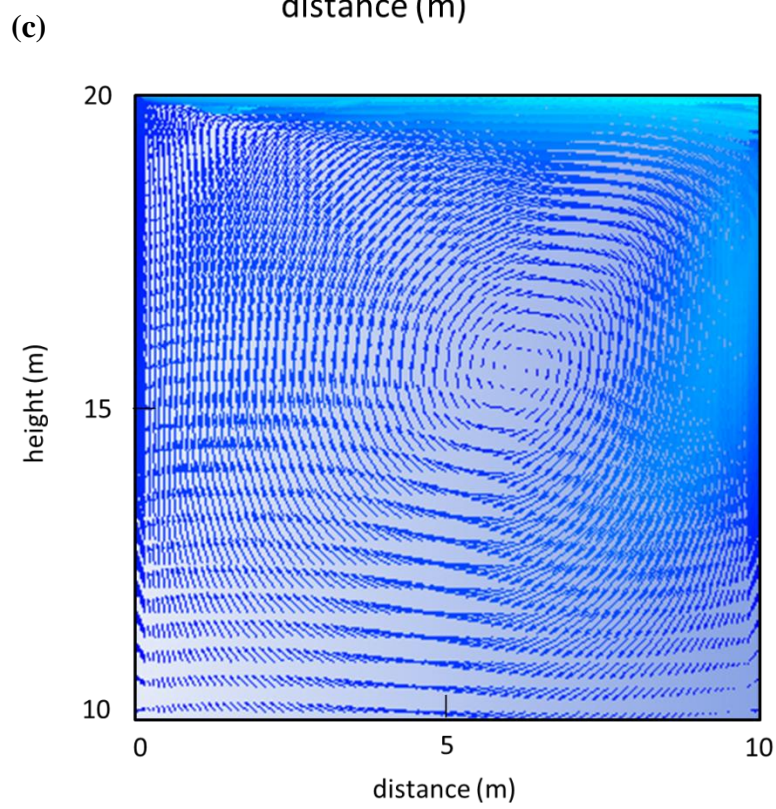
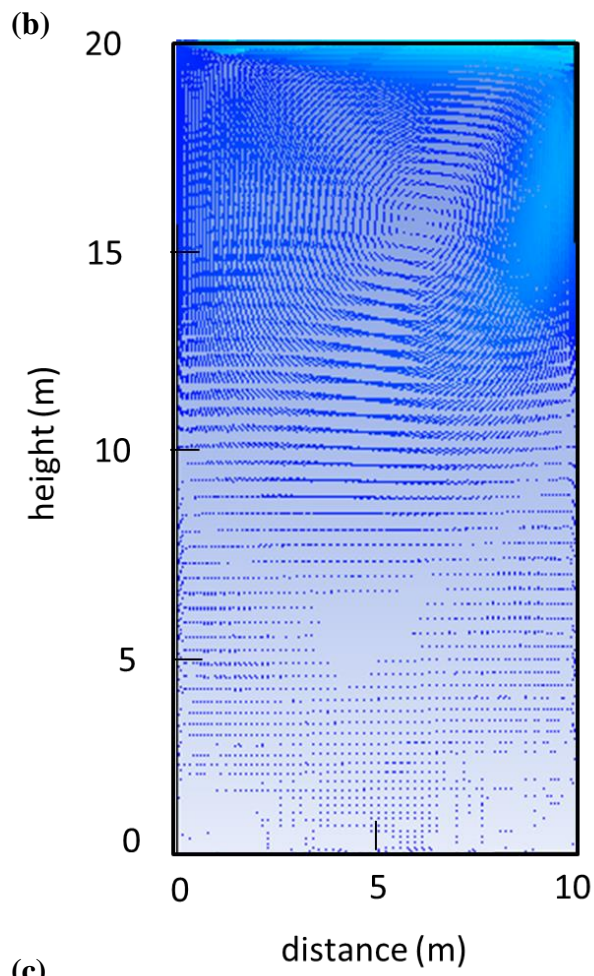


Figure 5 (a) Mass distribution with $\bar{D} = 369 \mu\text{m}$. (b) Number distribution with $\bar{D} = 369 \mu\text{m}$. (c) Mass distribution with $\bar{D} = 20 \mu\text{m}$. (d) Number distribution with $\bar{D} = 20 \mu\text{m}$.



(a)





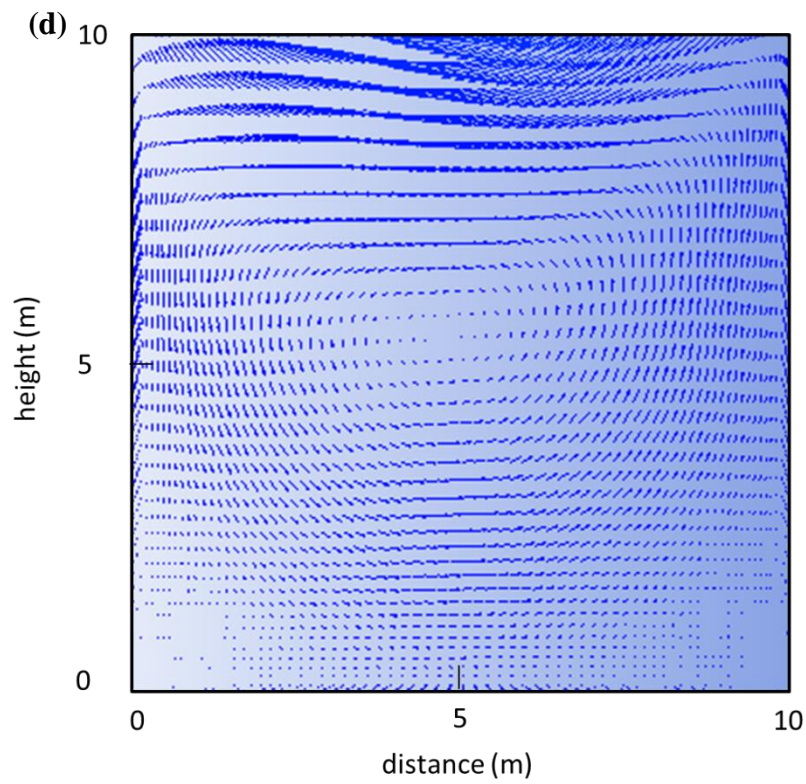


Figure 6 Velocity field in urban street canyon without spray system. (a) $H/W = 1$. (b) $H/W = 2$. (c) upper region of $H/W = 2$. (d) lower region of $H/W = 2$.

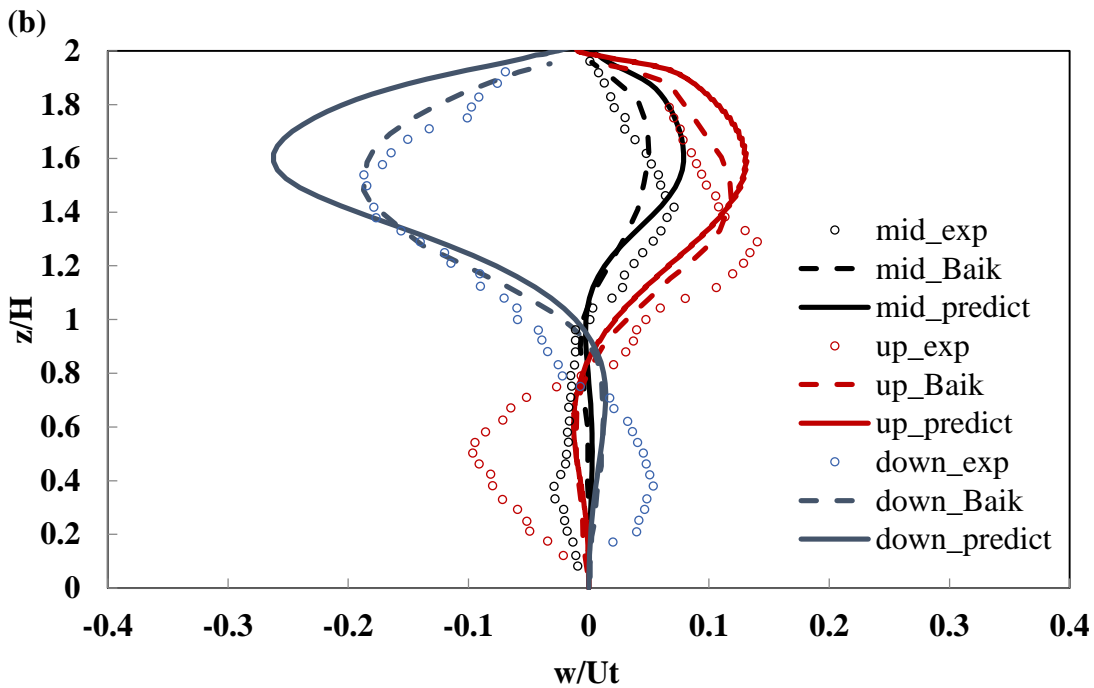
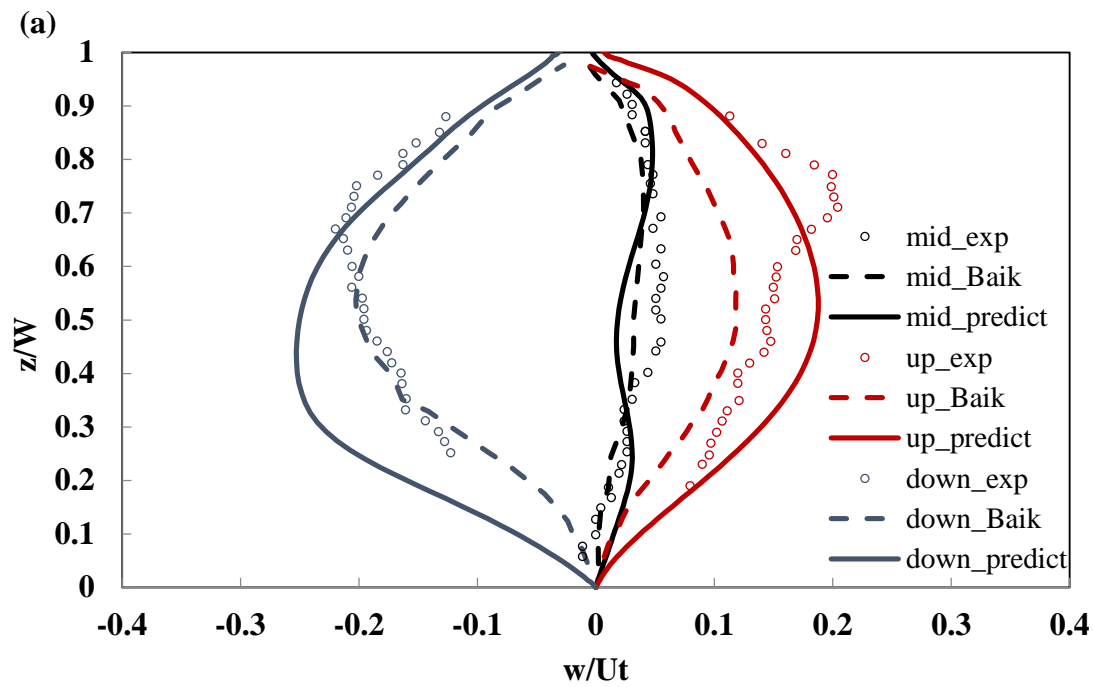


Figure 7 Normalized vertical velocity as a function of normalized height at an upstream position ($x/W = 0.125$), middle position ($x/W = 0.5$) and downstream position ($x/W = 0.875$). U_t is the x direction velocity just above the top of the building. (a) $H/W = 1$. (b) $H/W = 2$.

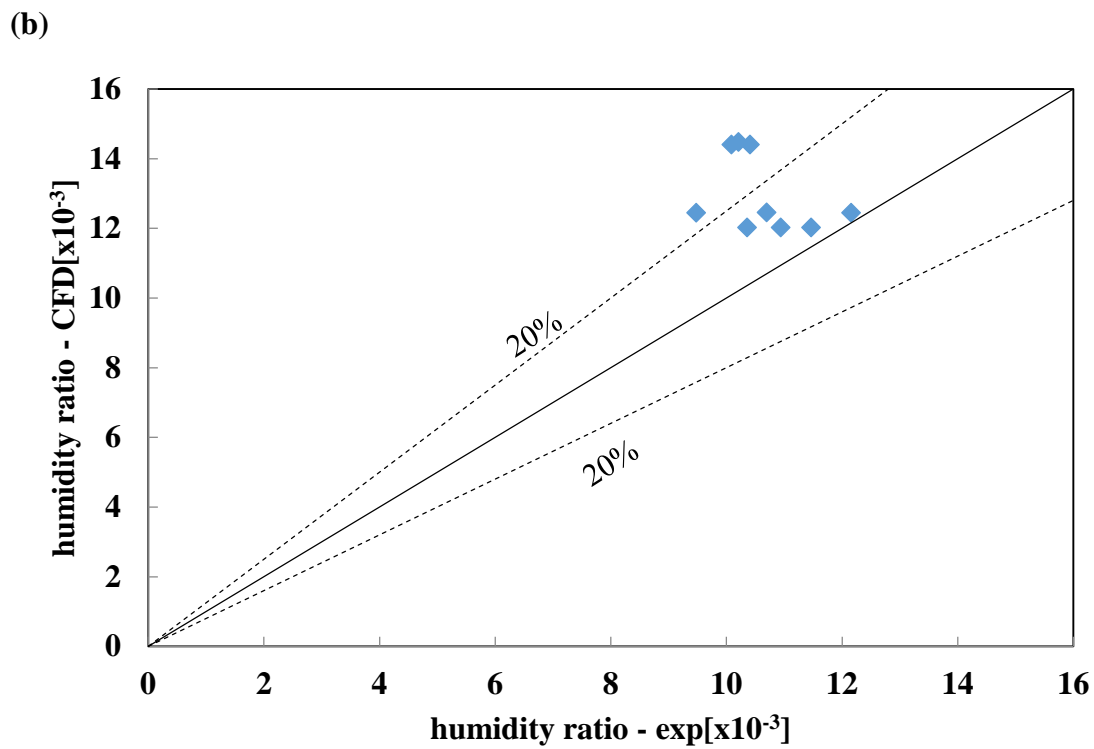
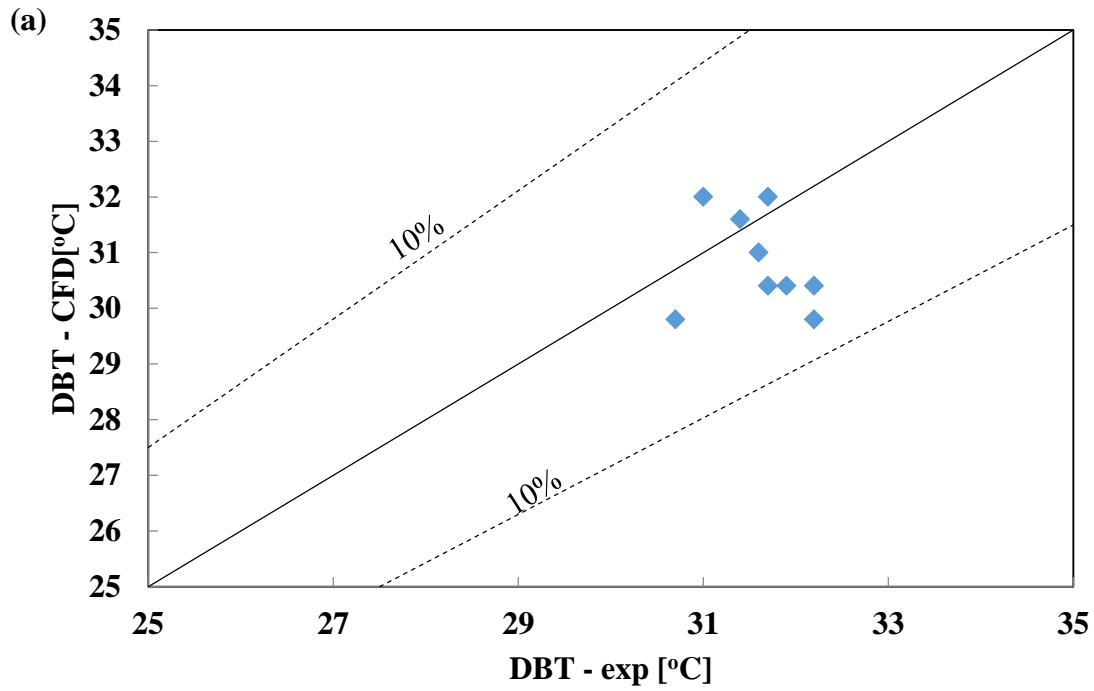
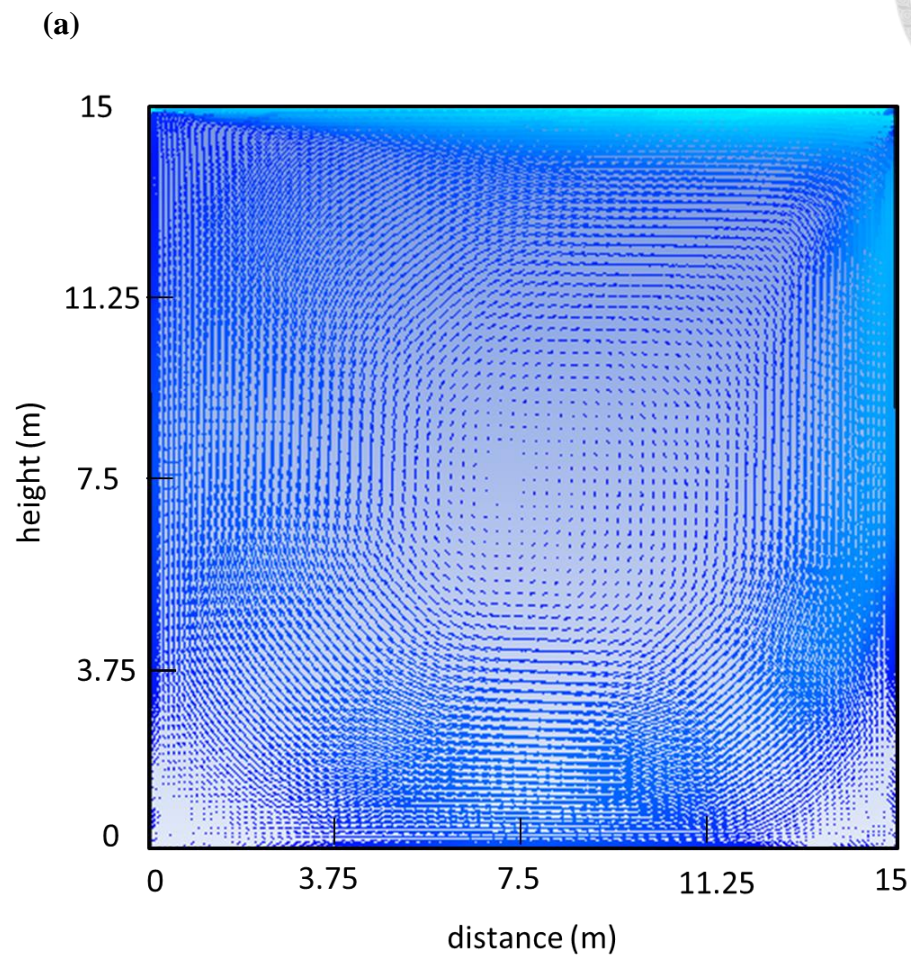
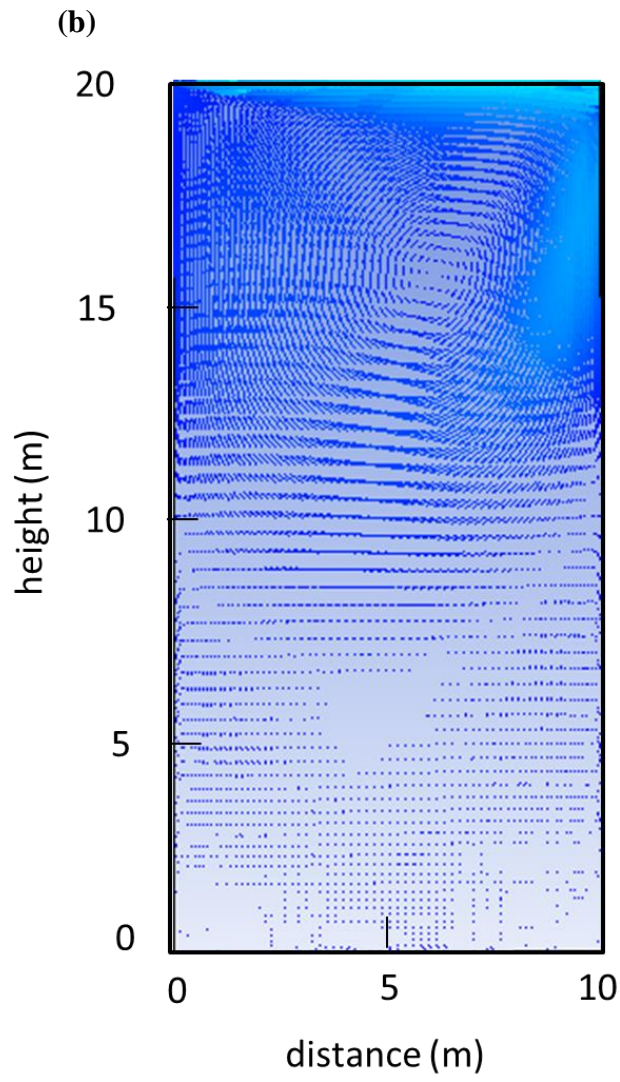
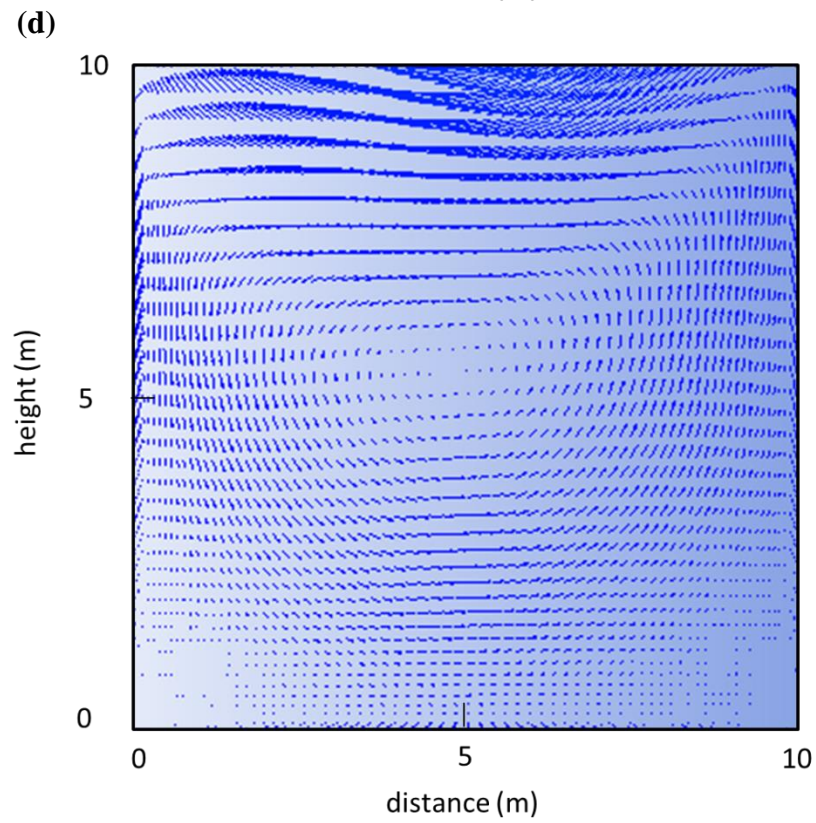
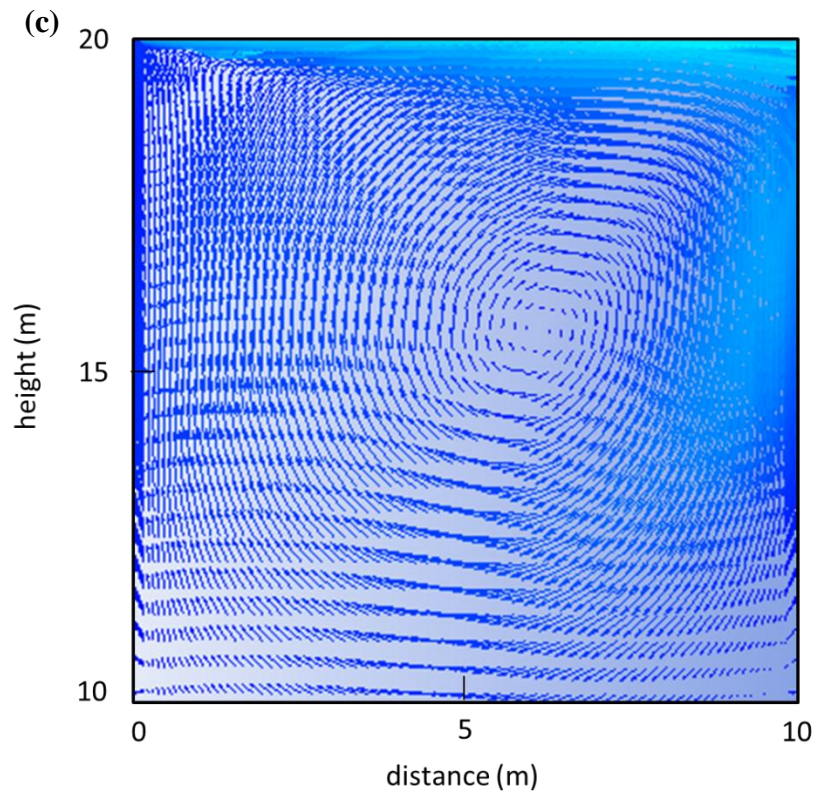


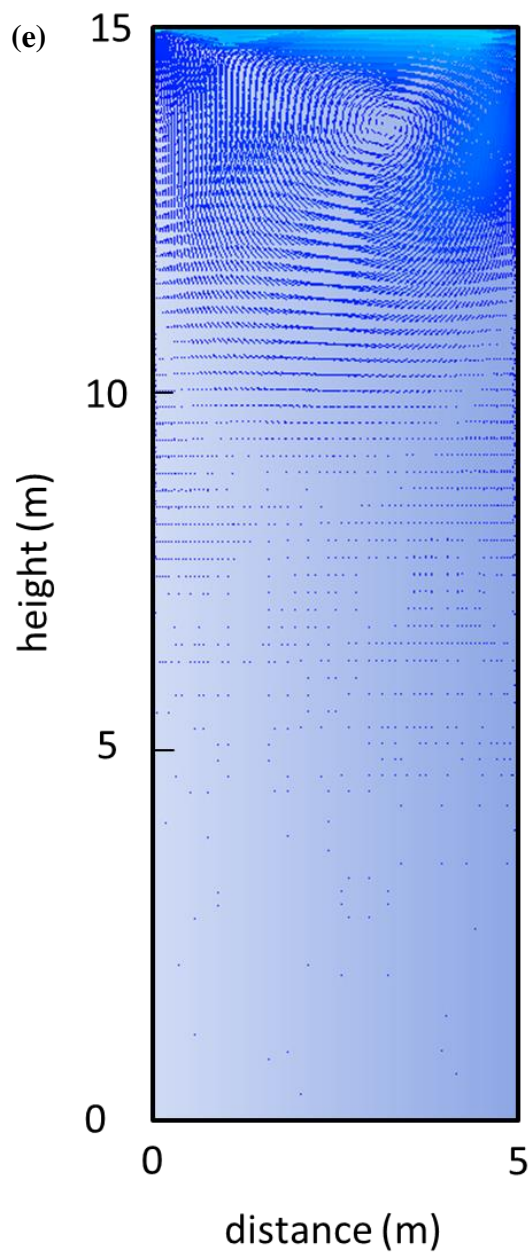
Figure 8 Comparison of calculated (CFD) and measured (exp) result. (a) DBT. (b)

humidity ratio.









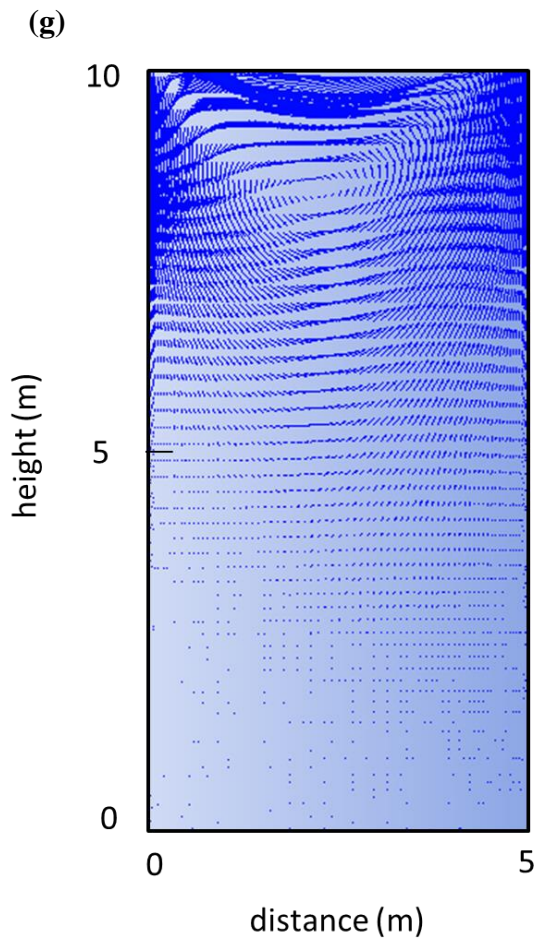
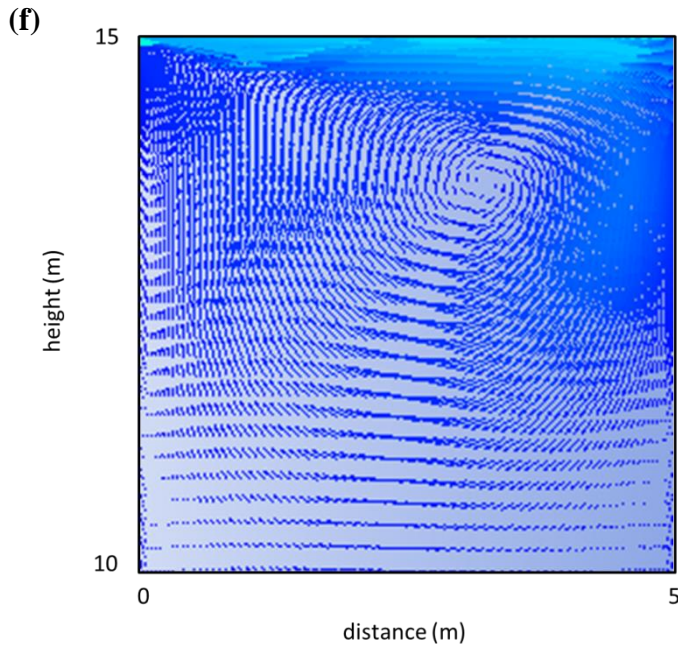
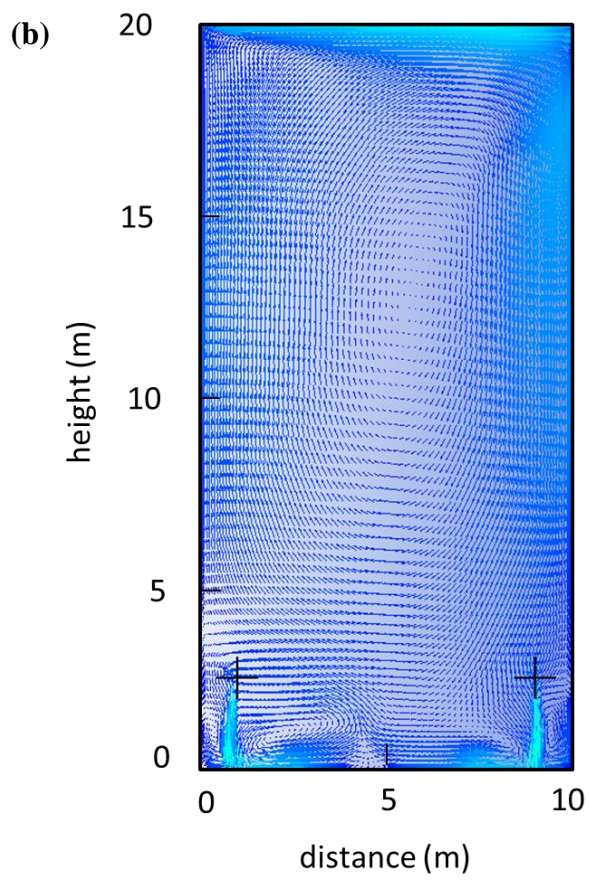
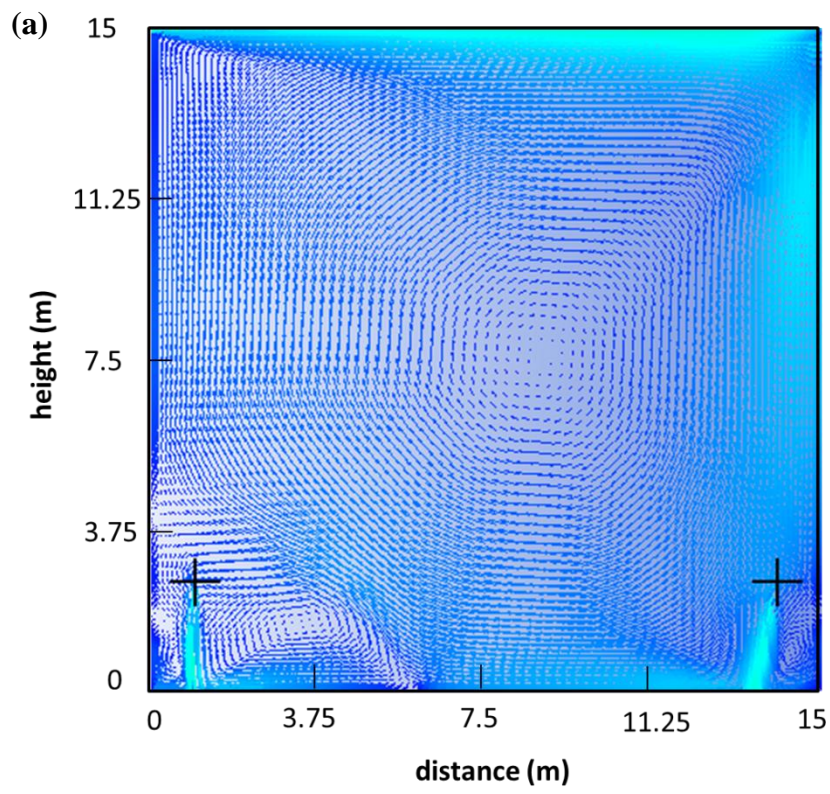


Figure 9 velocity field in the street canyon before spray systems operated. (a) $H/W = 1$. (b) $H/W = 2$. (c) upper region of $H/W = 2$. (d) lower region of $H/W = 2$. (e) $H/W = 3$. (f) upper region of $H/W = 3$. (g) lower region of $H/W = 3$.



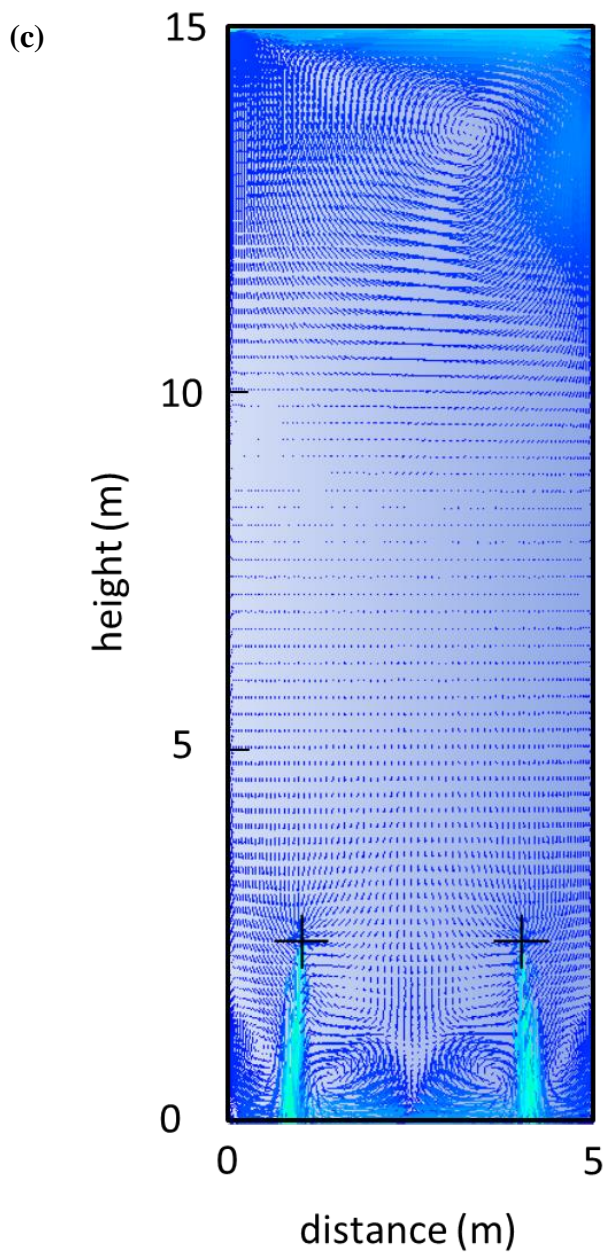
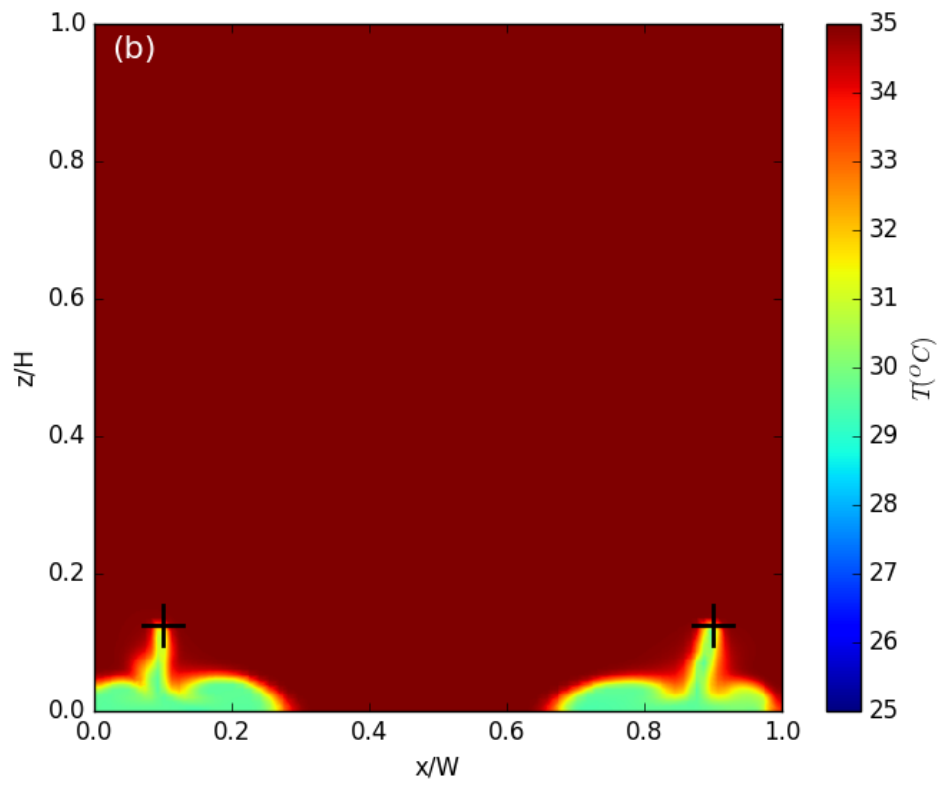
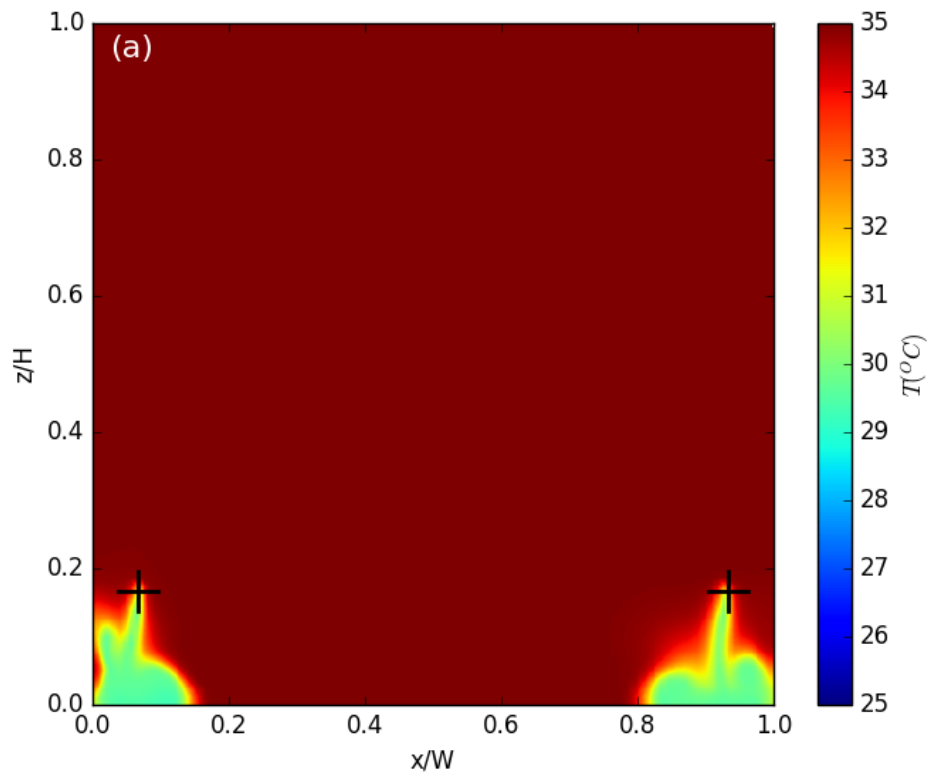
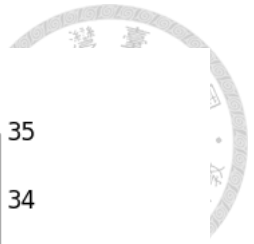


Figure 10 velocity field in the street canyon after spray systems operated. (a) $H/W = 1$.
(b) $H/W = 2$. (c) $H/W = 3$.



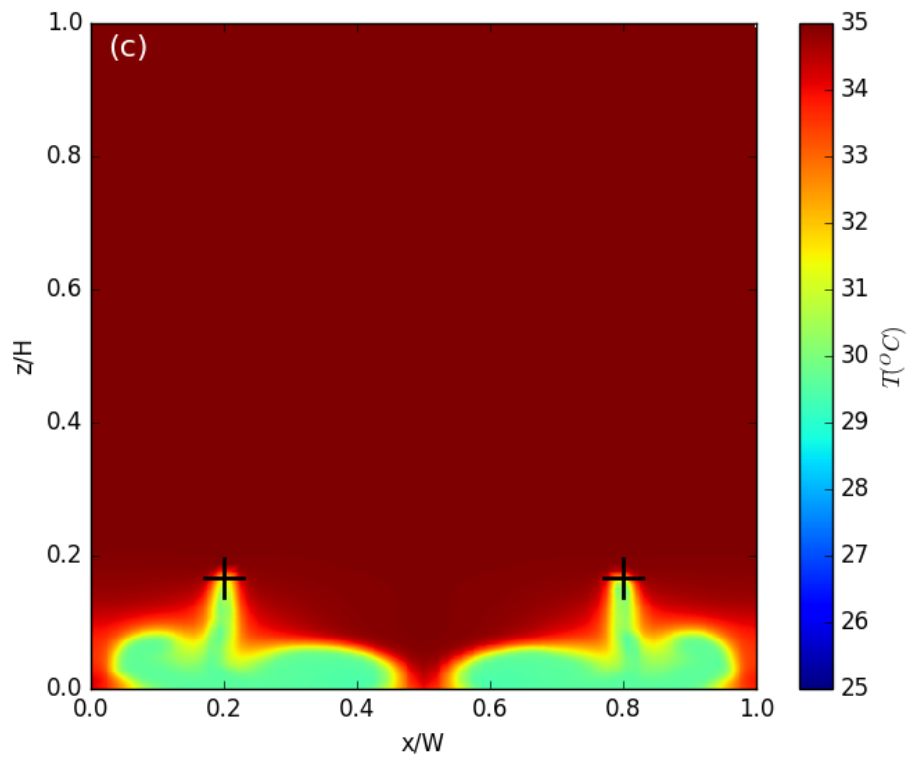
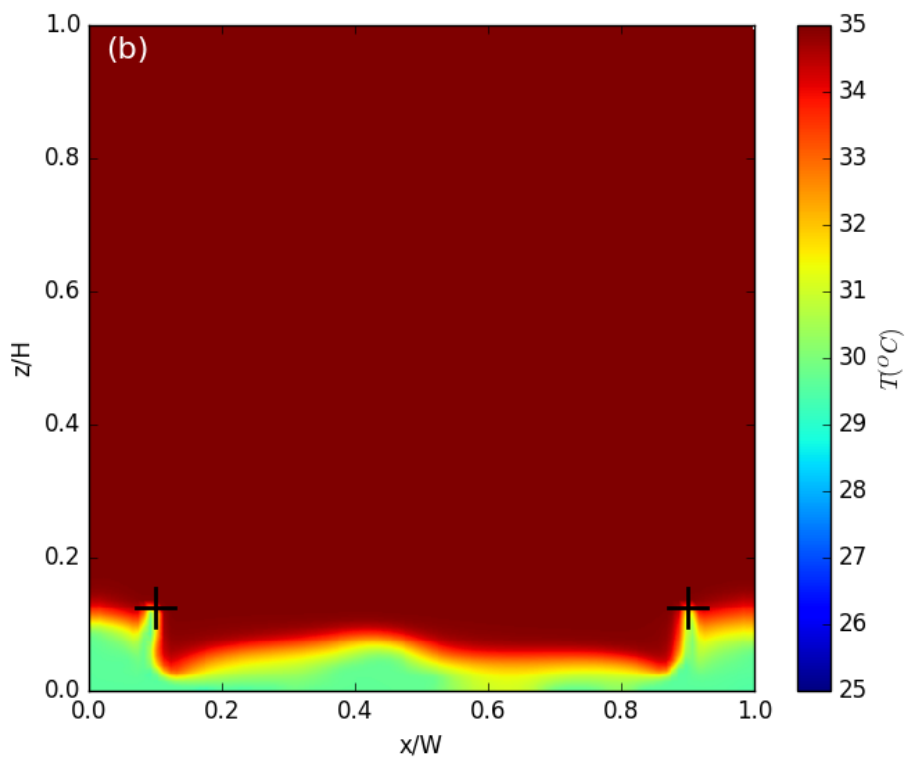
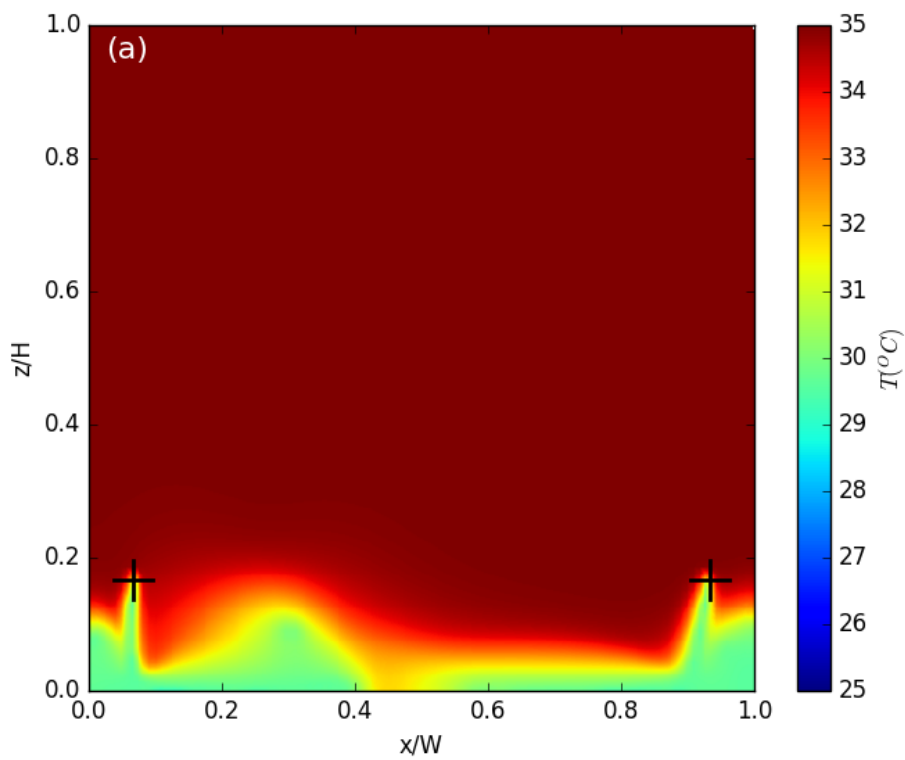
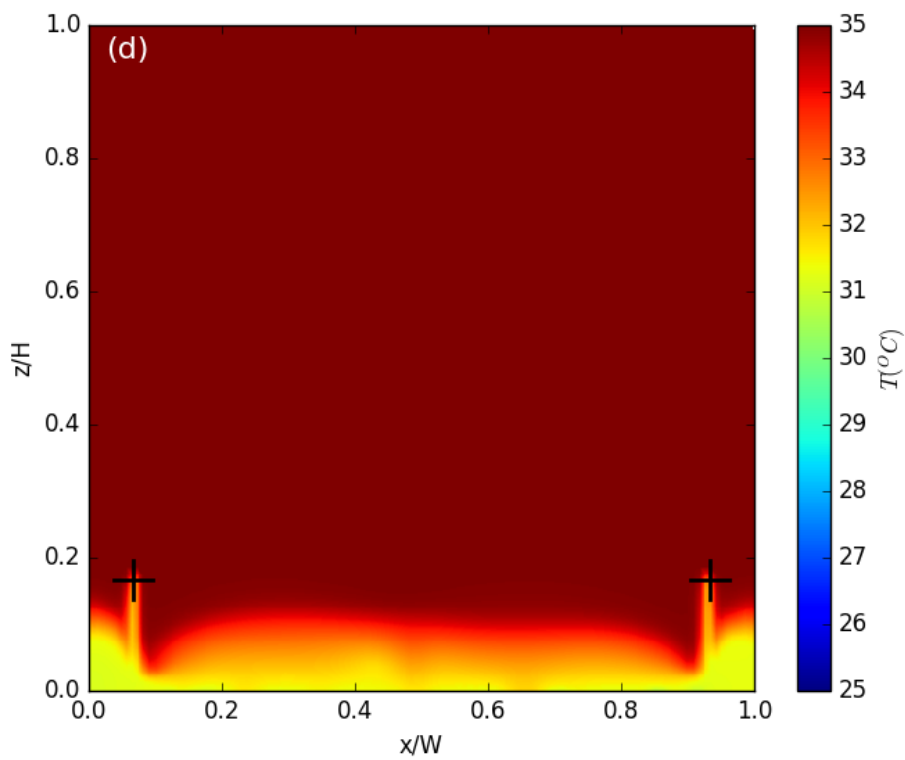
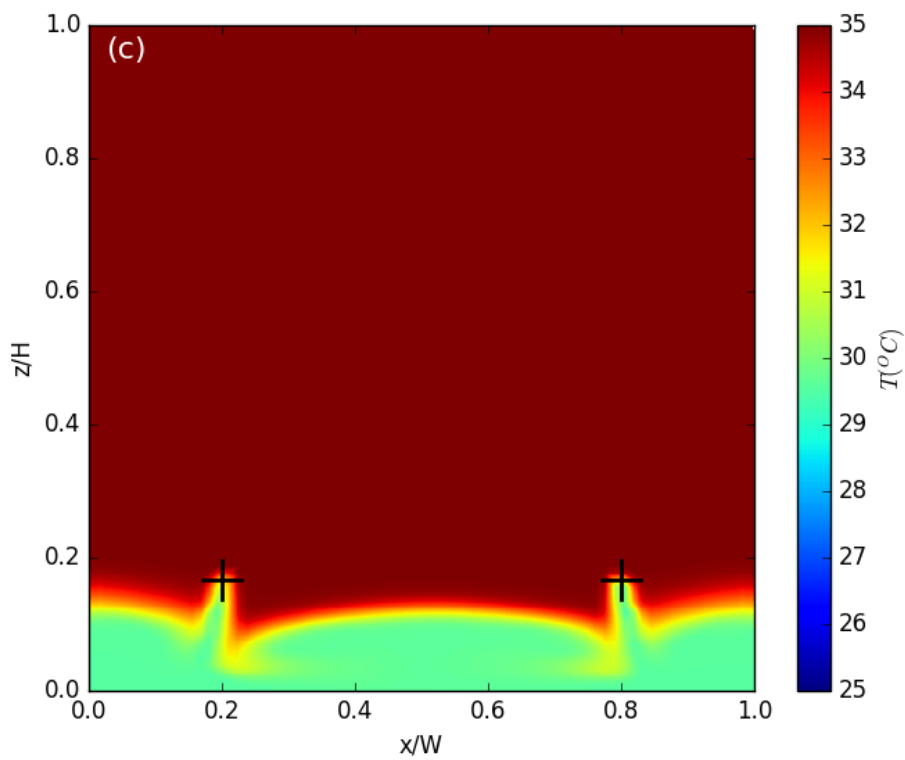


Figure 11 Temperature contours in the street canyon on the plane: $y = 0$ when $t = 5$ (sec)

The black cross indicates the position of water spray systems. (a) Case 1.1 ($H/W = 1$).

(b) Case 2.1 ($H/W = 2$). (c) Case 3.1 ($H/W = 3$).





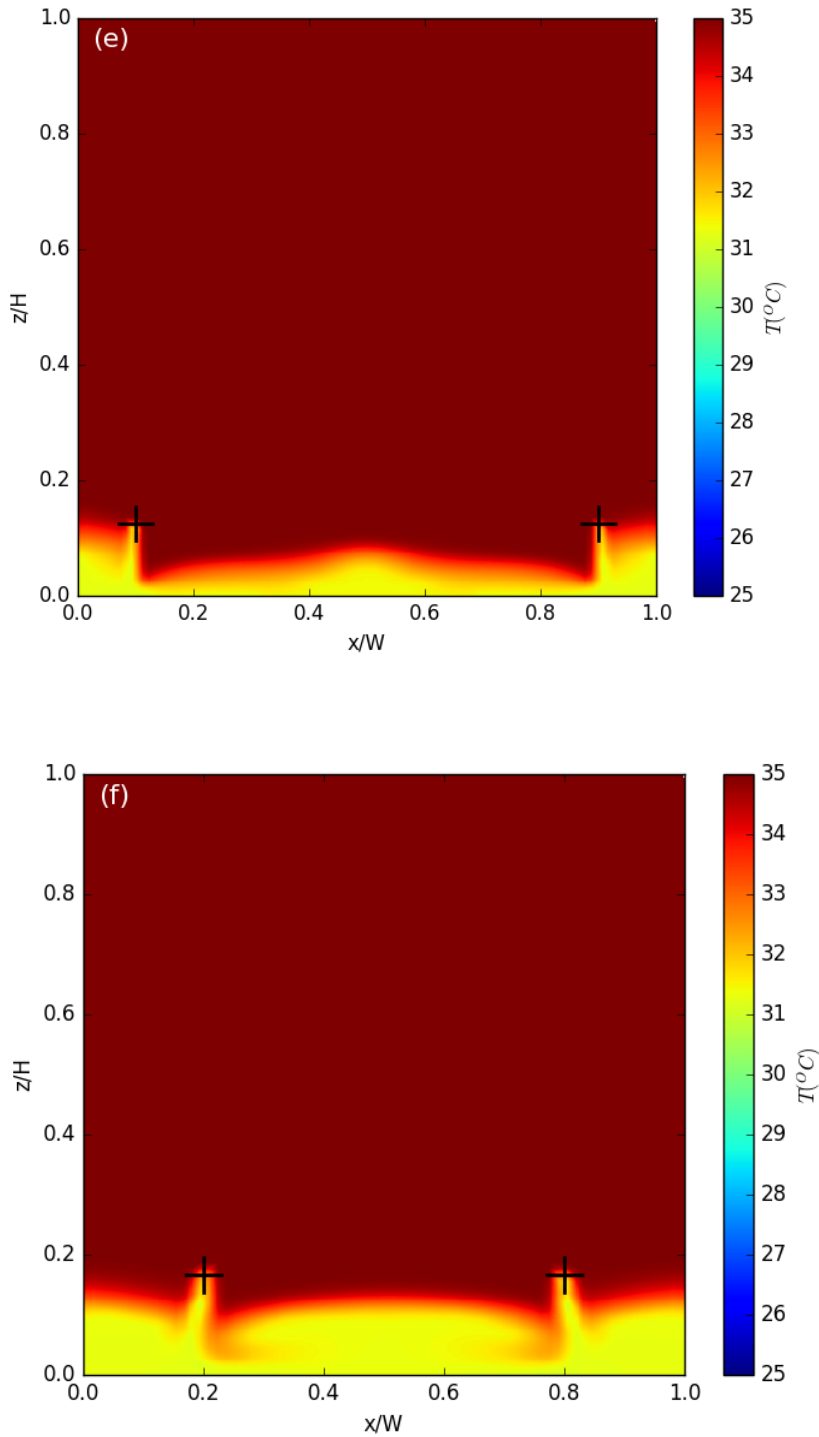


Figure 12 Temperature contours in the street canyon on the plane: $y = 0$ when steady state reached. The black cross indicates the position of water spray systems. (a) Case 1.1 ($H/W = 1$, $RH = 70\%$). (b) Case 2.1 ($H/W = 2$, $RH = 70\%$). (c) Case 3.1 ($H/W = 3$, $RH = 70\%$). (d) Case 1.2 ($H/W = 1$, $RH = 80\%$). (e) Case 2.2 ($H/W = 2$, $RH = 80\%$). (f) Case 3.2 ($H/W = 3$, $RH = 80\%$).

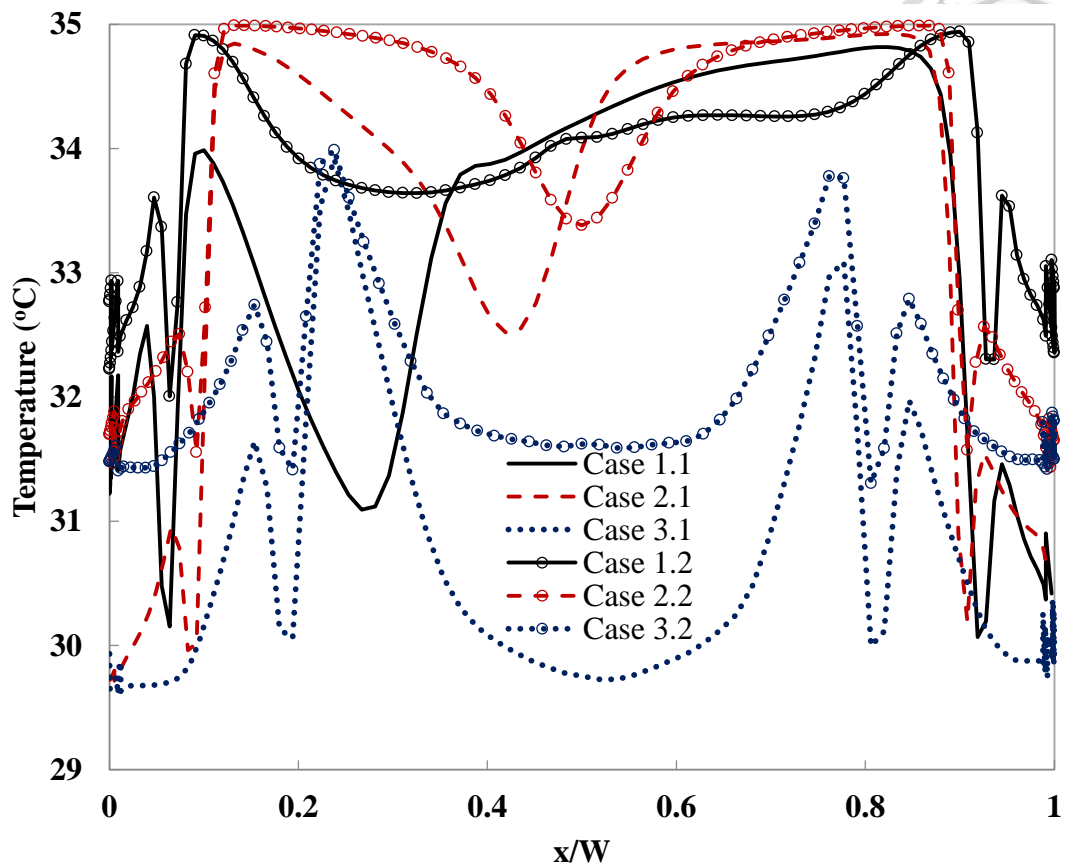


Figure 13 Temperature profile on the line: $y = 0$, $z = 1.5$ m with different aspect ratio and Relative humidity in Case 1.1 ($H/W = 1$, $RH = 70\%$), Case 2.1 ($H/W = 2$, $RH = 70\%$), Case 3.1 ($H/W = 3$, $RH = 70\%$), Case 1.2 ($H/W = 1$, $RH = 80\%$), Case 2.2 ($H/W = 2$, $RH = 80\%$), Case 3.2 ($H/W = 3$, $RH = 80\%$). The background temperature is $35\text{ }^{\circ}\text{C}$ and the normalized distance between the nozzles and building are 0.07, 0.1 and 0.2 for $H/W = 1, 2, 3$ respectively.

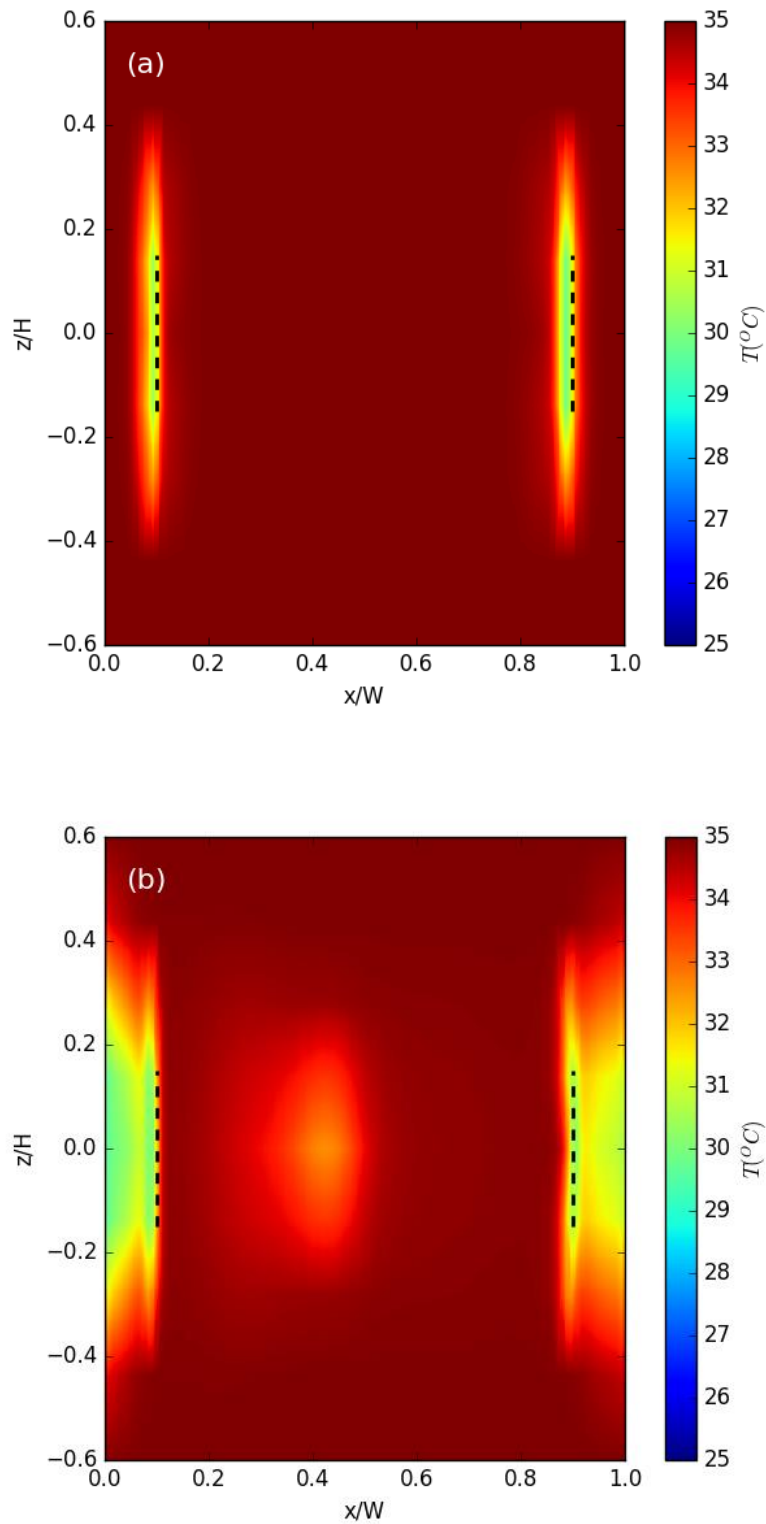


Figure 14 Temperature contour in Case 2.1 in the street canyon on x-y plane where height is 1.5 meters ($z = 1.5$). Dotted line shows the positions of spray nozzles (a) after 5 seconds. (b) after 12.5 seconds.

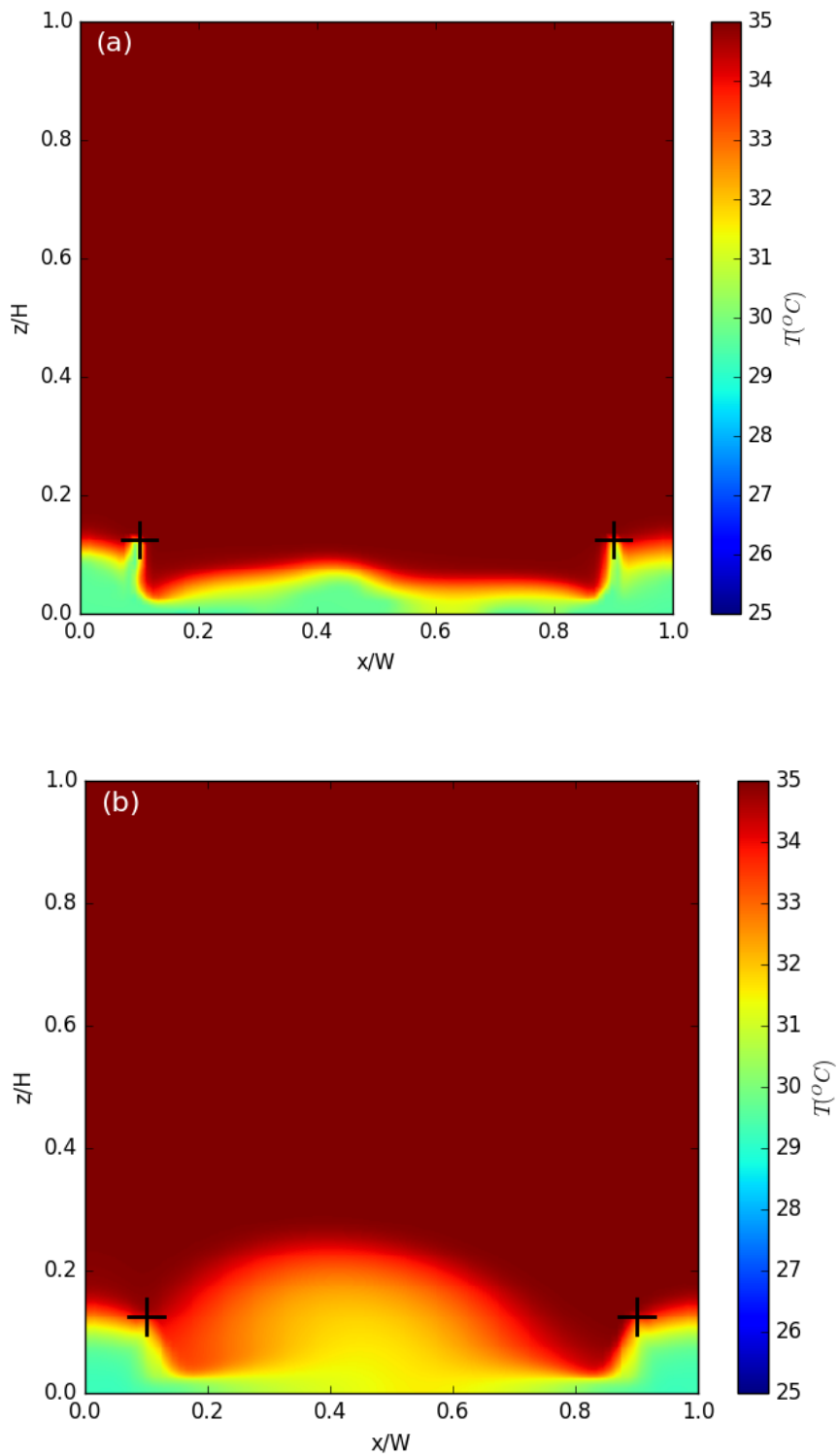


Figure 15 Temperature contours on the plane: $y = 0$. (a) Case 2.1 ($\bar{D} = 20 \mu\text{m}$). (b) Case 2.1.a ($\bar{D} = 40 \mu\text{m}$).

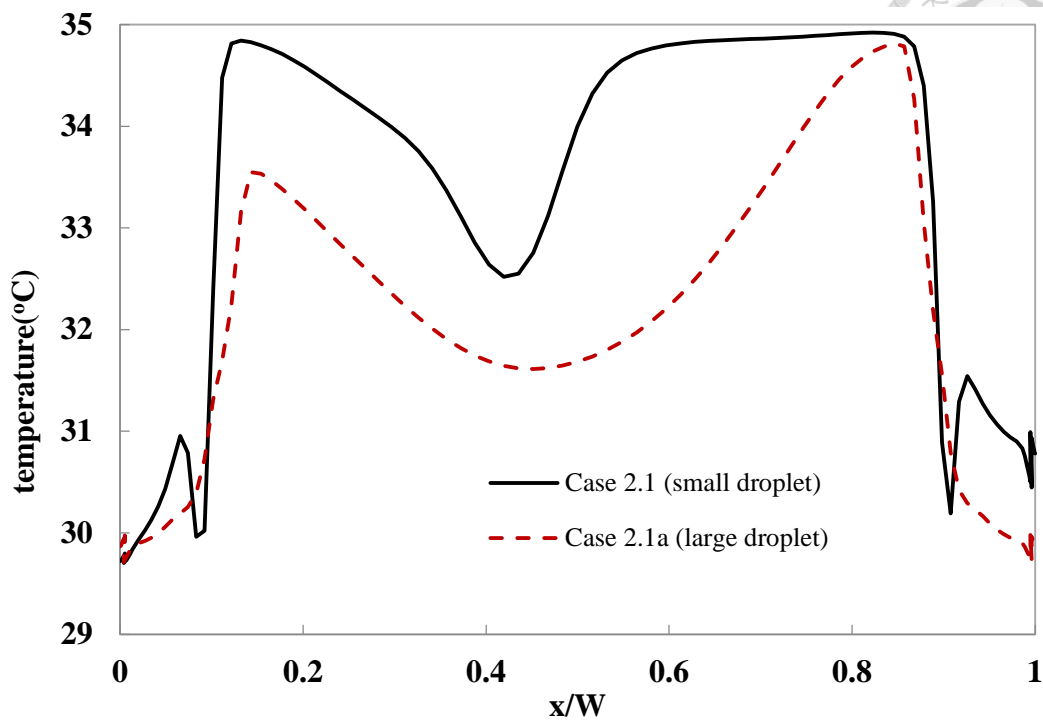


Figure 16 Temperature profile on the line: $y = 0$, $z = 1.5$ m, in Case 2.1 ($\bar{D} = 20\mu\text{m}$, $V_w = 15$ m/s, $\dot{m} = 0.01$ kg/s) and Case 2.1a ($\bar{D} = 369\mu\text{m}$, $V_w = 22$ m/s, $\dot{m} = 0.2$ kg/s). The background temperature is 35°C .

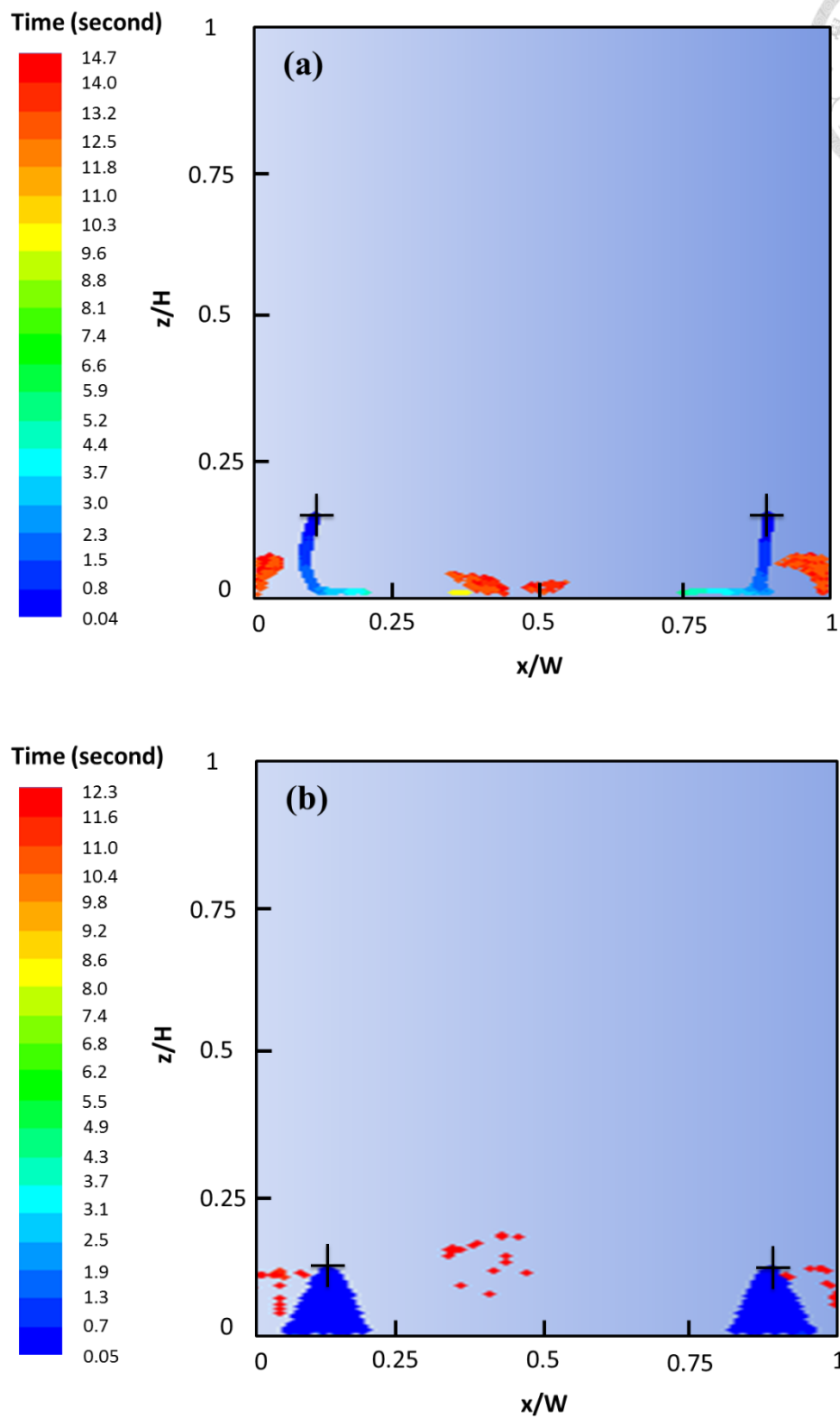
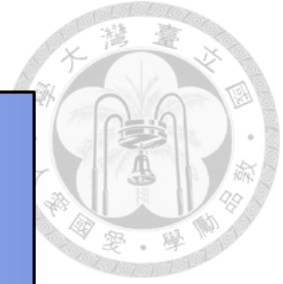


Figure 17 Residence time of droplet particles on the plane: $y = 0$. The black cross indicates the position of water spray systems. (a) Case 2.1 ($\bar{D} = 20 \mu\text{m}$). (b) Case 2.1a ($\bar{D} = 369 \mu\text{m}$).

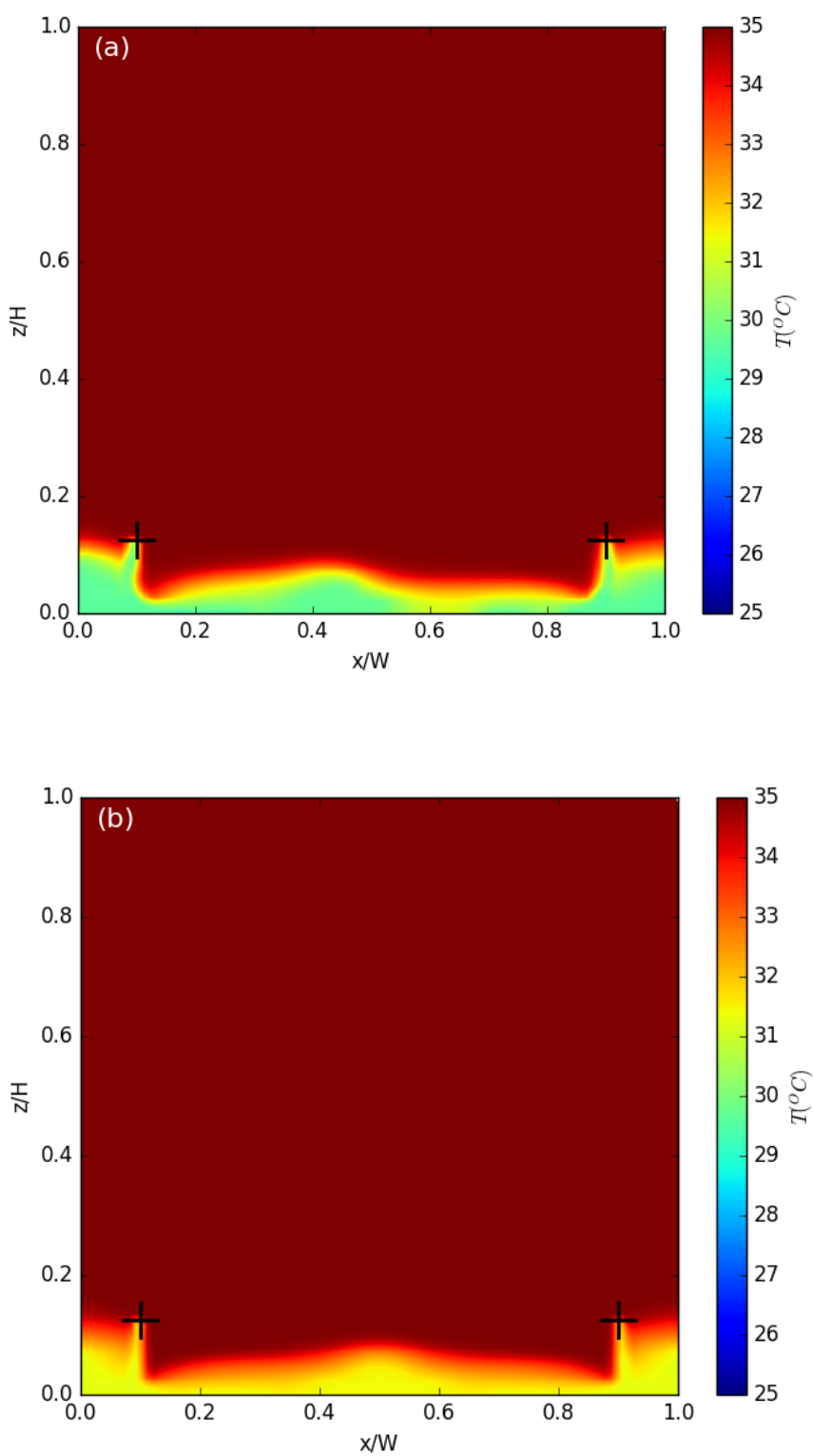
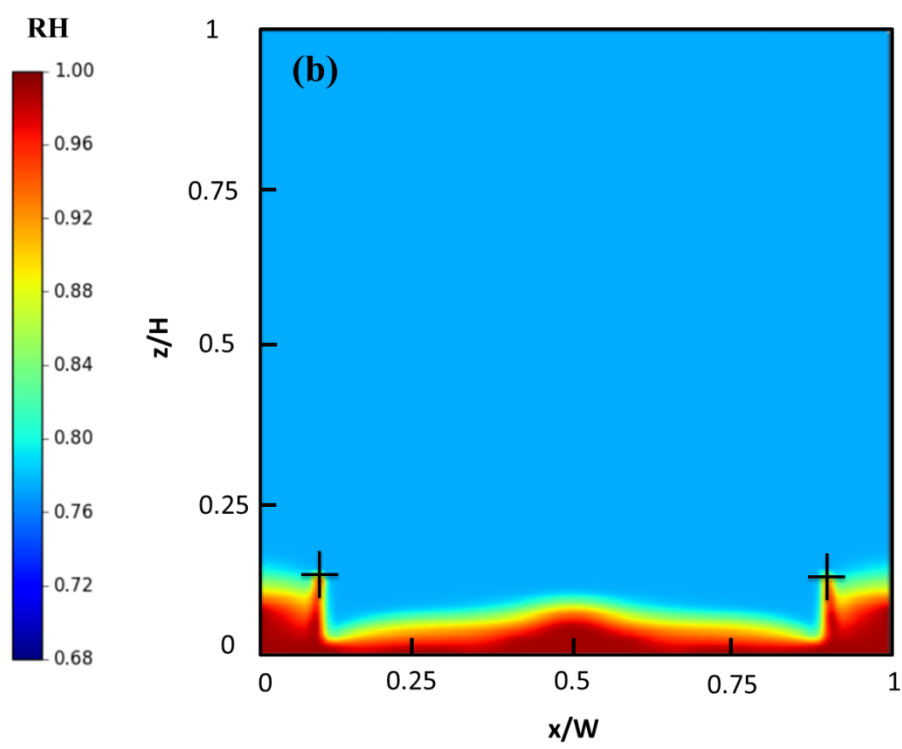
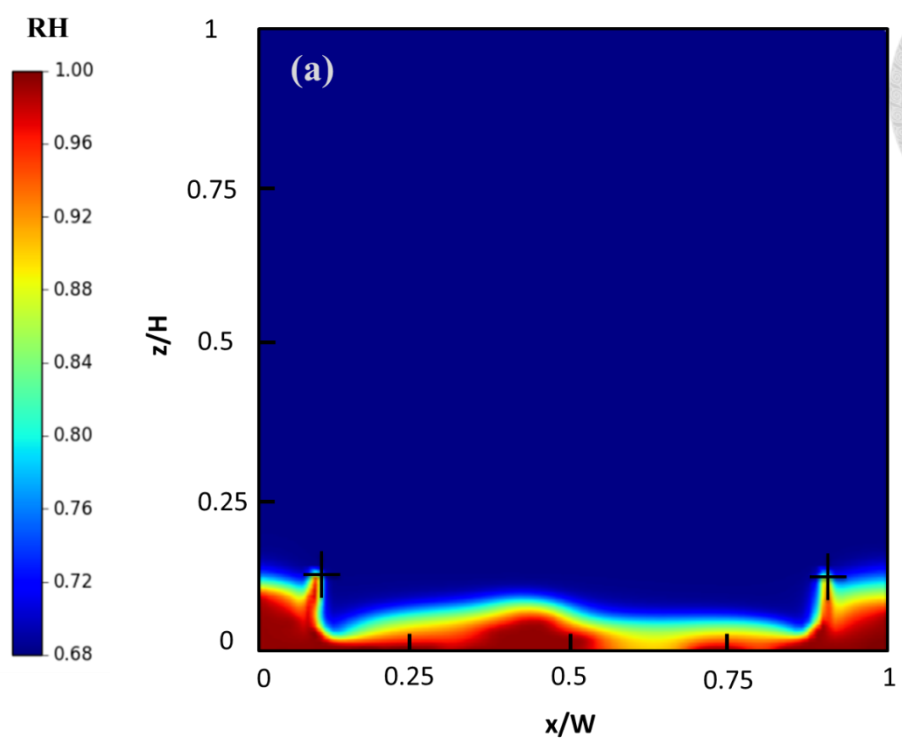


Figure 18 Temperature contours on the plane: $y = 0$. (a) Case 2.1 (RH = 70%). (b) Case 2.2 (RH = 80%).



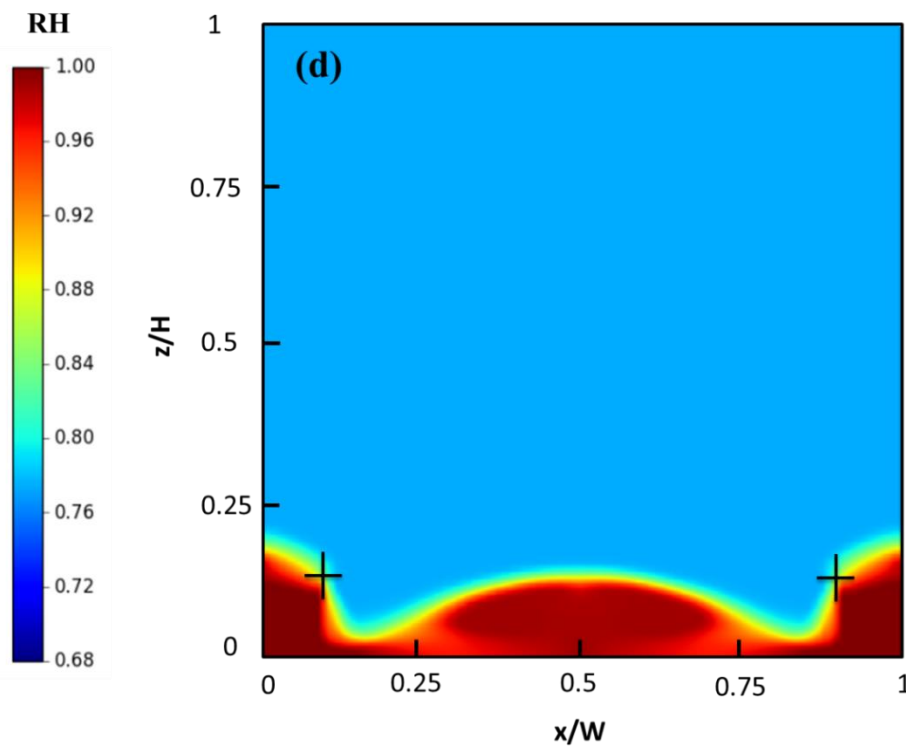
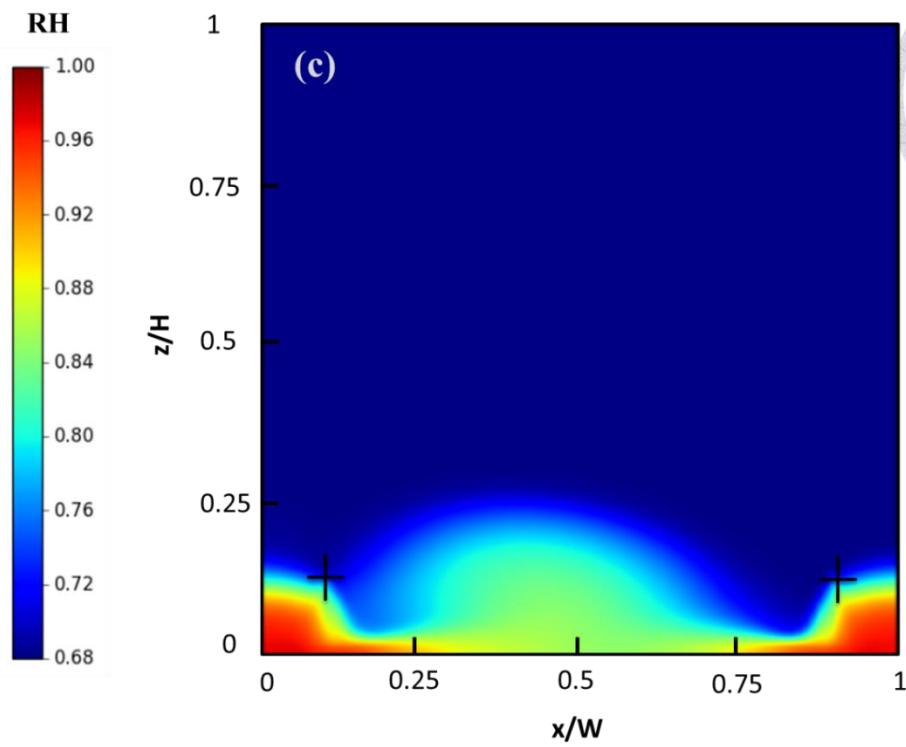


Figure 19 Relative humidity contours on the plane: $y = 0$. (a) Case 2.1 ($RH = 70\%$, $\bar{D} = 20 \mu\text{m}$). (b) Case 2.2 ($RH = 80\%$, $\bar{D} = 20 \mu\text{m}$). (c) Case 2.1a ($RH = 70\%$, $\bar{D} = 369 \mu\text{m}$). (d) Case 2.2a ($RH = 80\%$, $\bar{D} = 369 \mu\text{m}$).

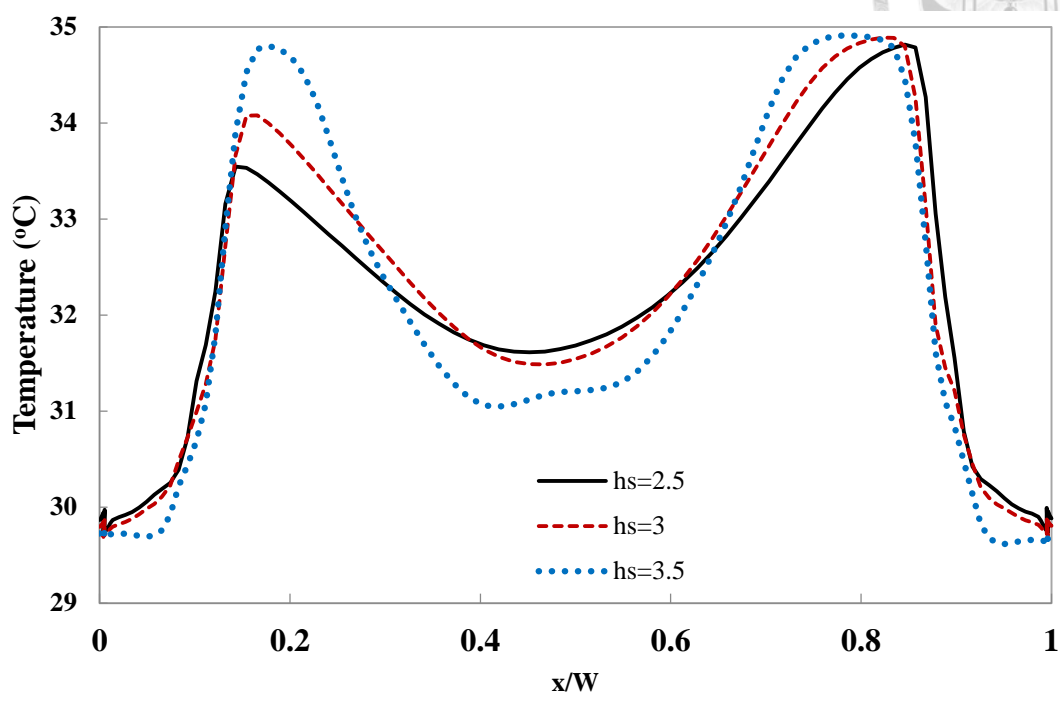
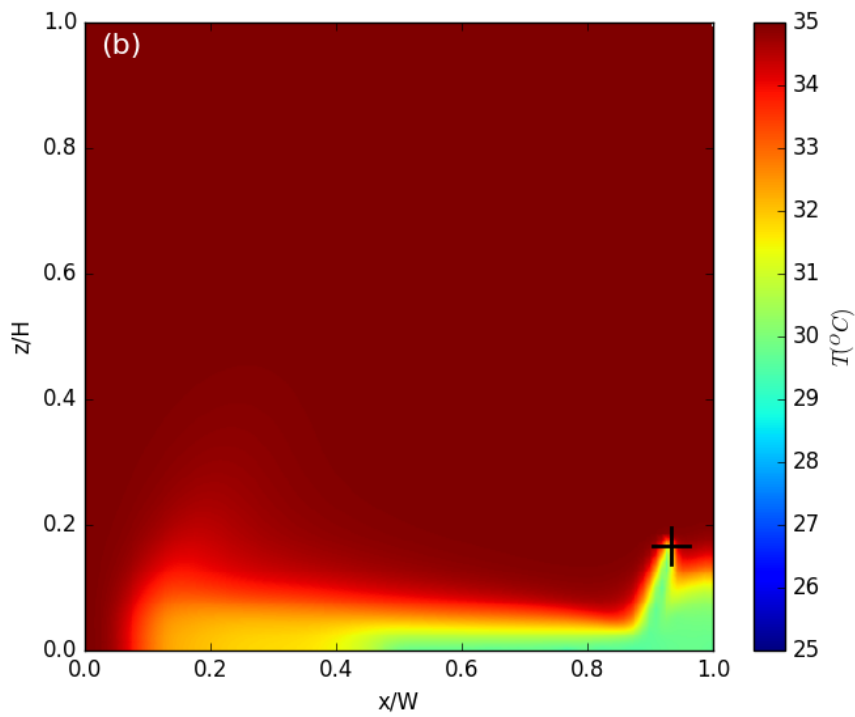
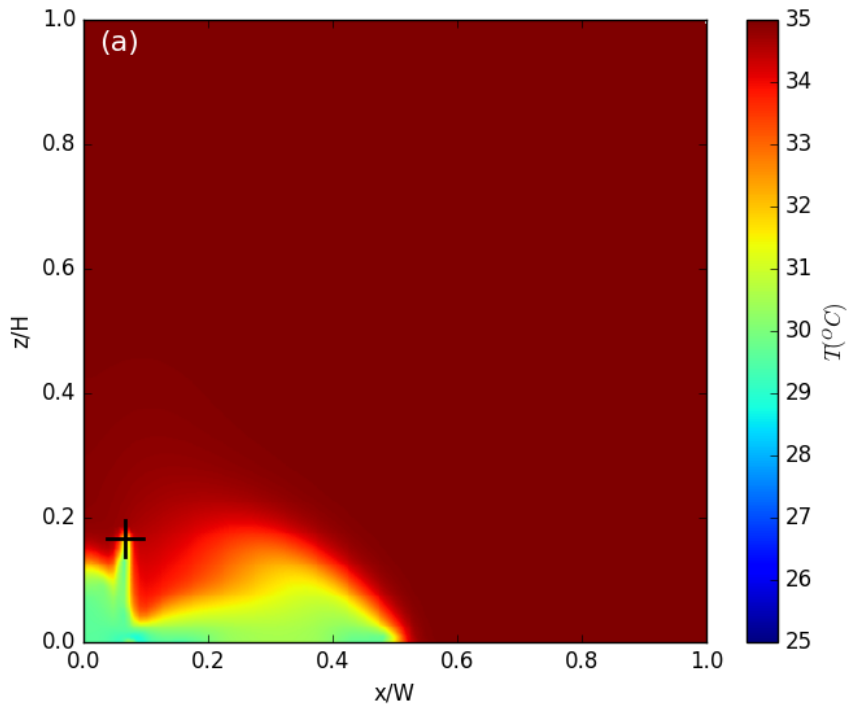


Figure 20 Temperature profiles on the line: $y = 0$, $z = 1.5$ m with different heights of spray nozzles ($h_s = 2.5, 3, 3.5$ m). The background temperature is 35°C .



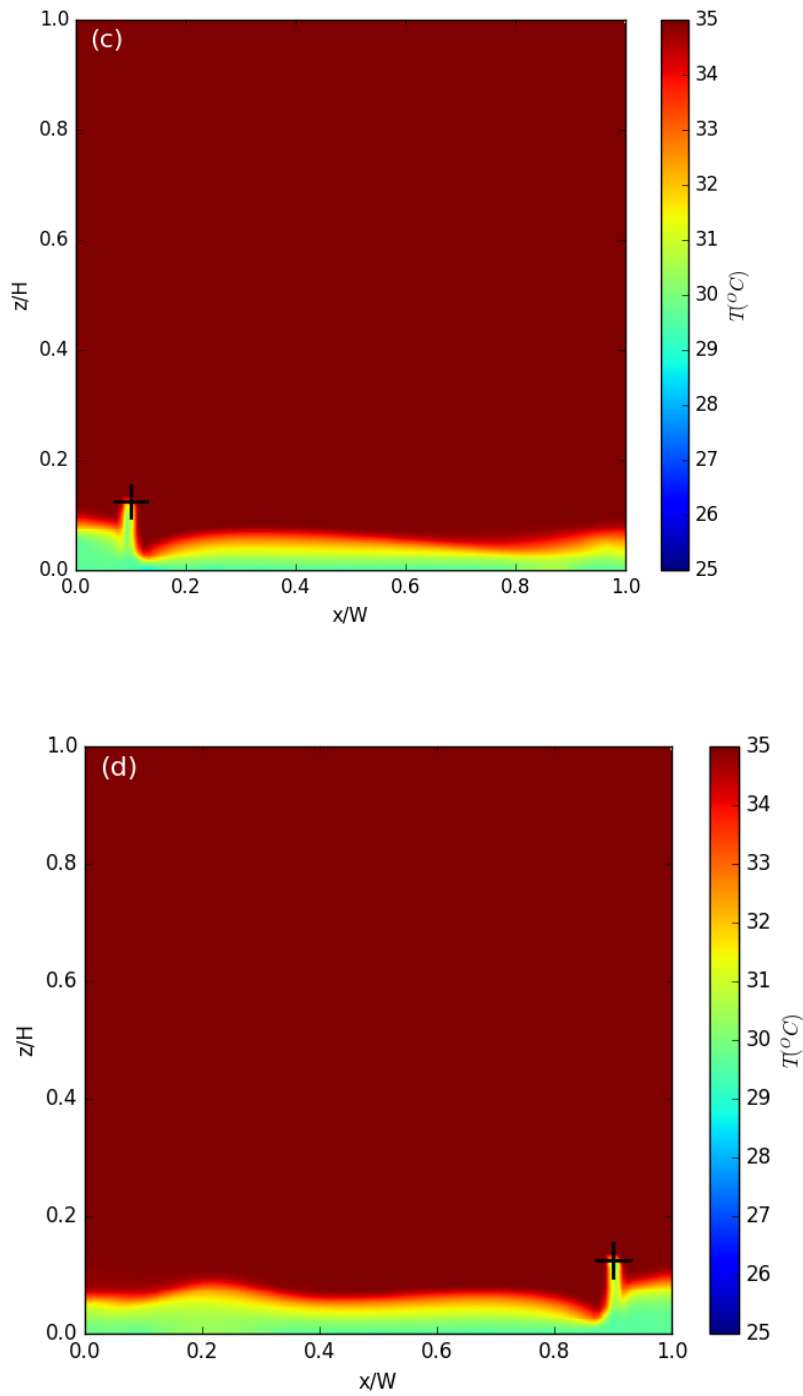


Figure 21 Temperature contours on the plane: $y = 0$. (a) Left side, $H/W = 1$. (b) Right side, $H/W = 1$. (c) Left side, $H/W = 2$. (d) Right side, $H/W = 2$.

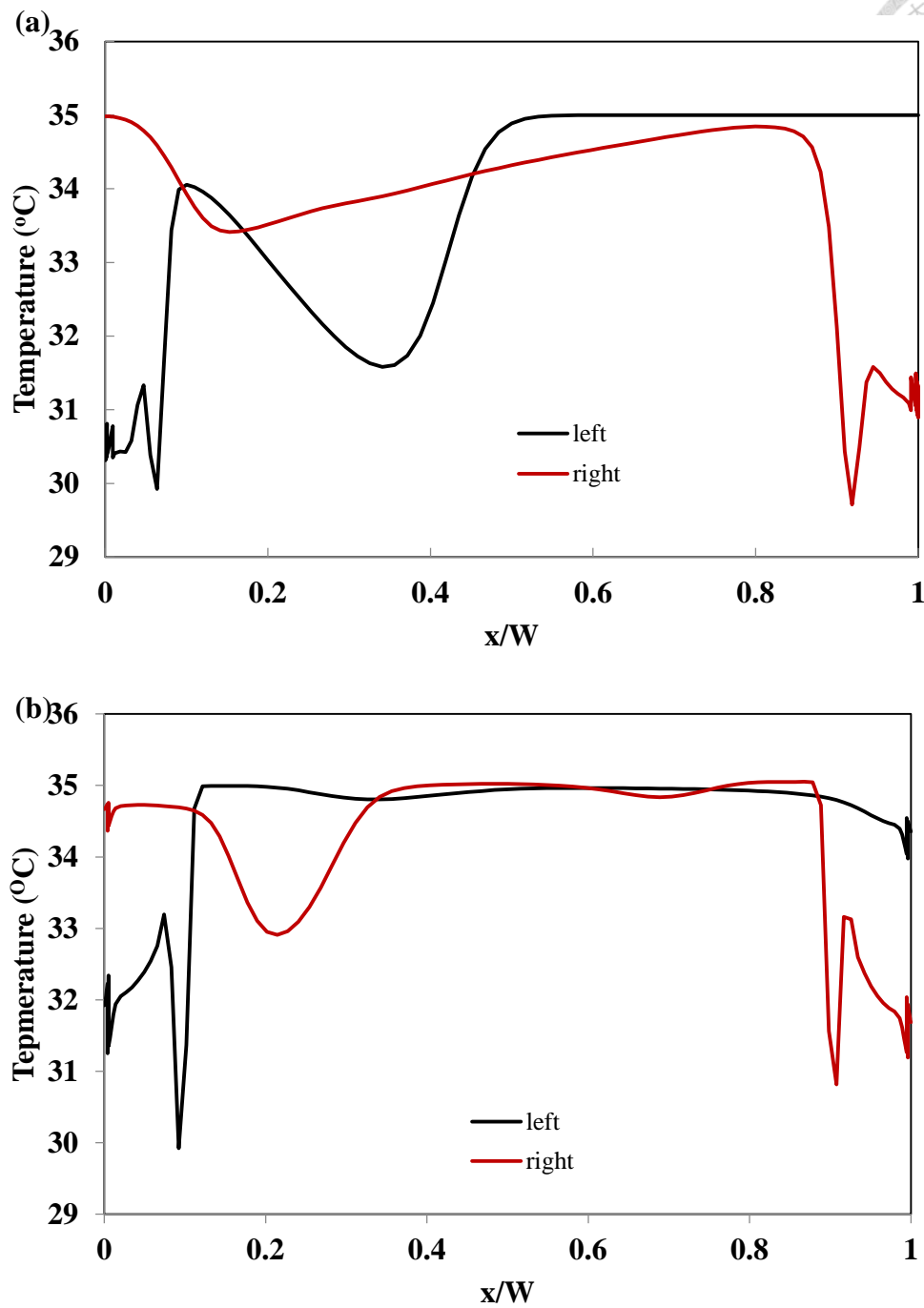
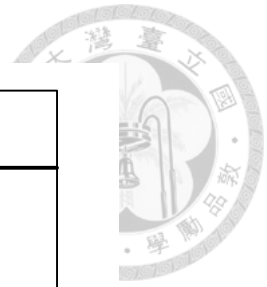
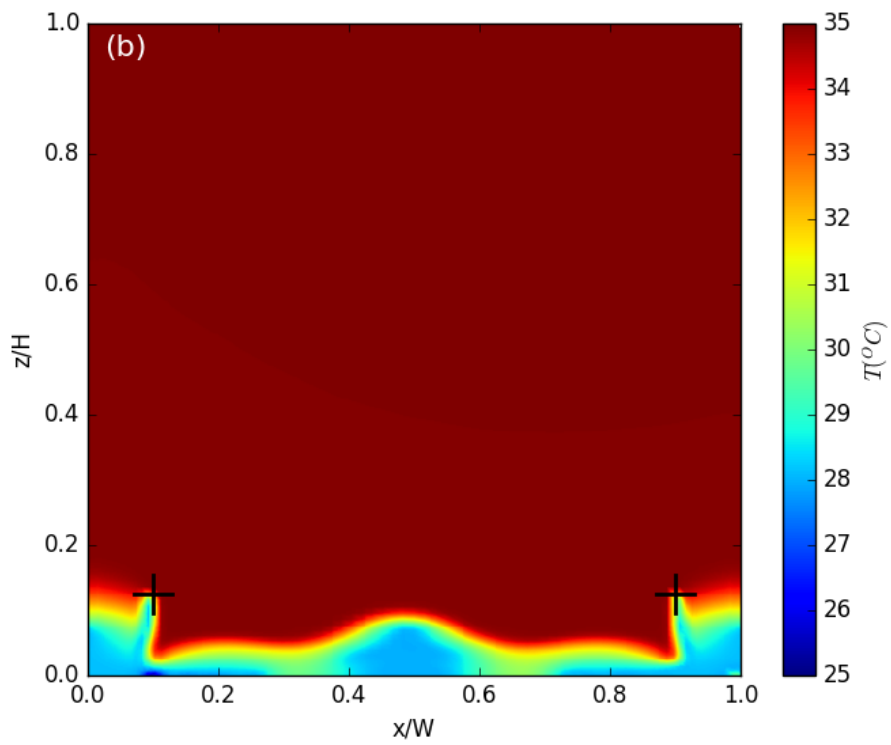
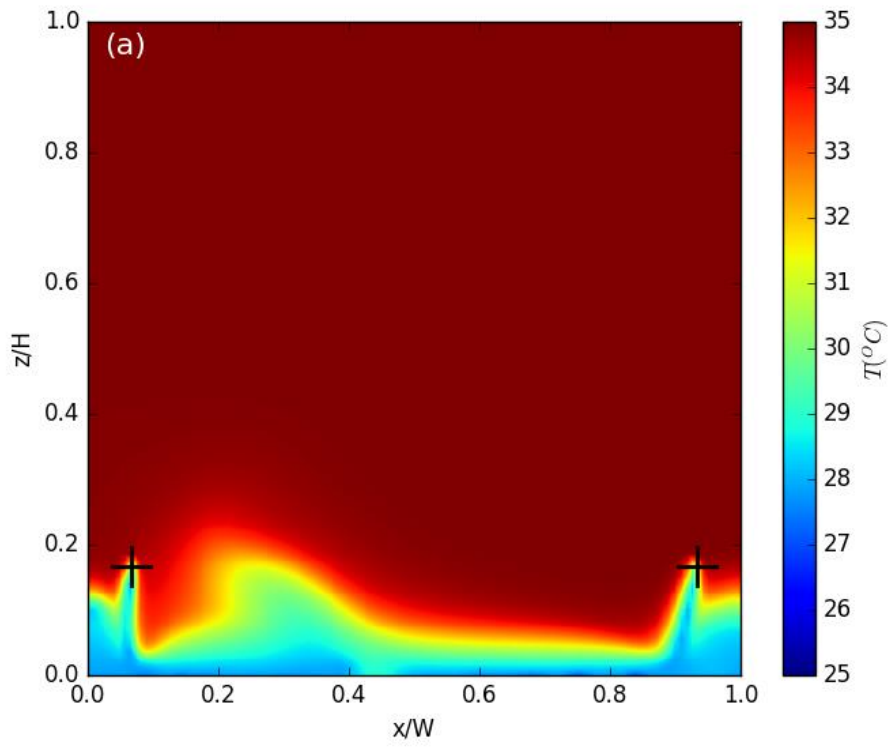


Figure 22 Temperature profiles on the line: $y = 0$, $z = 1.5$ m with spray nozzles wet on the left side or the right side. The background temperature is 35°C . (a) $H/W = 1$. (b) $H/W = 2$.



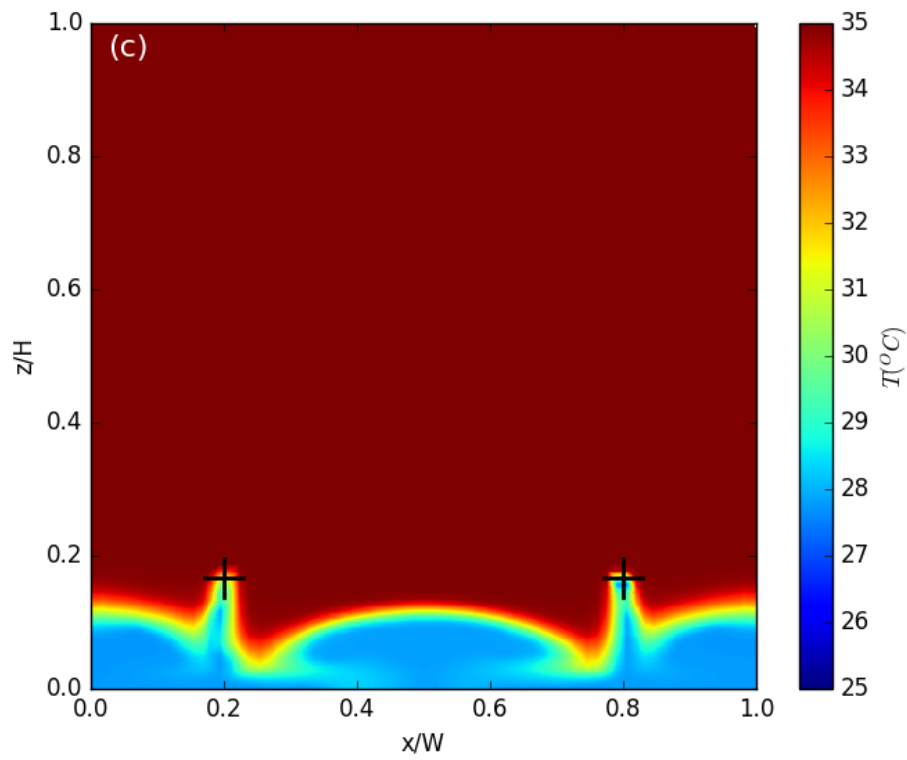


Figure 23 Temperature contours on the plane: $y = 0$ in the cases with $RH = 60\%$. (a)

$H/W = 1$. (b) $H/W = 2$. (c) $H/W = 3$.